AFAL TR-87-012

AD:

(12)

Final Report
for the period
1 October 1982 to
31 October 1986

Pulsed Inductive Thruster Component Technology

April 1987

Authors:
C. L. Dailey
R. H. Lovberg

TRW, Inc.
One Space Park
Redondo Beach, CA 90278

F04611-82-C-0058

Approved for Public Release

prepared for the: **Air Force Astronautics Laboratory**

Air Force Space Technology Center
Space Division, Air Force Systems Command
Edwards Air Force Base,
California 93523-5000

NOTICE

When U.S. Government drawings, specifications, or other data are used for any purpose other than a definitely related Government procurement operation, the fact that the Government may have formulated, furnished, or in any way supplied the said drawings, specifications, or other data, is not to be regarded by implication or otherwise, or in any way licensing the holder or any other person or corporation, or conveying any rights or permission to manufacture, use, or sell any patented invention that may be related thereto.

FOREWORD

This report describes the work accomplished by TRW under contract F04611-82-C-0058 with the Air Force Rocket Propulsion Laboratory (AFRPL), Edwards Air Force Base, California. AFRPL Project Managers were Major G. D. Nordley and Captains M. R. Brasher, J. B. Elledge, and O. W. Kilgore.

This report has been reviewed and is approved for release and distribution in accordance with the distribution statement on the cover and on the DD Form 1473.

Robert J. Vondra
ROBERT J. VONDRA
Project Manager

Edward S. Huston
EDWARD S. HUSTON, MAJOR, USAF
Chief, Advanced Propulsion Branch

FOR THE COMMANDER

Edward L. Ibbotson
EDWARD L. IBBOTSON, Lt Col, USAF
Dep Chief, Liquid Rocket Division

A181068

SECURITY CLASSIFICATION OF THIS PAGE

REPORT DOCUMENTATION PAGE

1a. REPORT SECURITY CLASSIFICATION UNCLASSIFIED	1b. RESTRICTIVE MARKINGS
2a. SECURITY CLASSIFICATION AUTHORITY	3. DISTRIBUTION/AVAILABILITY OF REPORT Approved for Public Release. Distribution is Unlimited.
2b. DECLASSIFICATION/DOWNGRADING SCHEDULE	
4. PERFORMING ORGANIZATION REPORT NUMBER(S)	5. MONITORING ORGANIZATION REPORT NUMBER(S) AFAL-TR-87-012
6a. NAME OF PERFORMING ORGANIZATION TRW, Inc. 6b. OFFICE SYMBOL (If applicable)	7a. NAME OF MONITORING ORGANIZATION Air Force Astronautics Laboratory
6c. ADDRESS (City, State and ZIP Code) One Space Park Redondo Beach, CA 90278	7b. ADDRESS (City, State and ZIP Code) AFAL/LKCJ Edwards Air Force Base, CA 93523-5000
8a. NAME OF FUNDING/SPONSORING ORGANIZATION 8b. OFFICE SYMBOL (If applicable)	9. PROCUREMENT INSTRUMENT IDENTIFICATION NUMBER F04611-82-C-0058
8c. ADDRESS (City, State and ZIP Code)	10. SOURCE OF FUNDING NOS.

PROGRAM ELEMENT NO.	PROJECT NO.	TASK NO.	WORK UNIT NO.
62302F	5730	00	LD

11. TITLE (Include Security Classification) PULSED INDUCTIVE THRUSTER COMPONENT TECHNOLOGY (U)

12. PERSONAL AUTHOR(S)
Dailey, C. L., and Lovberg, R. H.

13a. TYPE OF REPORT	13b. TIME COVERED	14. DATE OF REPORT (Yr., Mo., Day)	15. PAGE COUNT
Final	FROM 82/10/1 TO 86/10/31	87/4	82

16. SUPPLEMENTARY NOTATION

17. COSATI CODES			18. SUBJECT TERMS (Continue on reverse if necessary and identify by block number)
FIELD	GROUP	SUB. GR.	Electric Propulsion, Pulsed Inductive Thruster (PIT), Magnetic Plasma Accelerator.
21	03		

19. ABSTRACT (Continue on reverse if necessary and identify by block number)

The Pulsed Inductive Thruster (PIT) is an electrical propulsion device that accelerates a plasma propellant by the JxB Lorentz force, and in which the driving current in the plasma is induced, rather than being introduced through electrodes. This program

This component technology program has addressed: thruster circuit component design; plasma probe diagnostics and thrust balance measurements for two of the three thruster designs developed during the program; design of a flight-type capacitor, capacitor pad life testing, and demonstration of the system in the clamped discharge mode. A numerical simulation of thruster operation was developed and used to elucidate the effects on efficiency of circuit parameters, plasma conductiveity and scale size.

Capacitor test results indicate very long life is obtainable with modest voltage derating using paper/polypropylene capacitors. Development of a successful scheme for high-power, high frequency diode clamping has made it possible to operate without significant

over

20. DISTRIBUTION/AVAILABILITY OF ABSTRACT	21. ABSTRACT SECURITY CLASSIFICATION
UNCLASSIFIED/UNLIMITED ☐ SAME AS RPT. ☒ DTIC USERS ☐	UNCLASSIFIED

22a. NAME OF RESPONSIBLE INDIVIDUAL	22b. TELEPHONE NUMBER (Include Area Code)	22c. OFFICE SYMBOL
Robert J. Vondra	(805) 275-5473	LKCJ

DD FORM 1473, 83 APR   EDITION OF 1 JAN 73 IS OBSOLETE.

SECURITY CLASSIFICATION OF THIS PAGE

Block 19 (continued): capacitor voltage reversal, and hence to extend capacitor life by up to two orders of magnitude.

A life demonstration of the propellant injection valve exceeded the goal of one million cycles; however, a rotary device may be better suited for the Pulsed Inductive Thruster.

PIT Plasma probe diagnostics were helpful in understanding thruster operation. Both current density and magnetic field probes showed the need for testing with a larger vacuum chamber to thruster coil diameter ratio, and with a stronger induced electric field to ionize and drive the plasma current. Keywords: Magnetic plasma accelerator, Electric propulsion,

TABLE OF CONTENTS

Table of Contents (Continued)

1. INTRODUCTION

This Pulsed Inductive Thruster (PIT) report was prepared by the Engineering Operations organization of TRW's Applied Technology Division. It documents the results of a four-year program performed under AFRPL Contract No. F04611-82-C-0058 to analyze and demonstrate the concept feasibility for an advanced technology high thrust electric propulsion system capable of meeting Air Force primary space propulsion requirements.

The Pulsed Inductive Thruster is an electrical propulsion device that accelerates a plasma propellant by the JxB Lorentz force, and in which the driving current in the plasma is induced, rather than being introduced through electrodes.

The TRW propulsion organization has been actively involved in research and development of this thruster concept under Air Force sponsorship since 1962. TRW management regards this innovative propulsion technology as potentially useful for orbital transfer of very large masses required by both Strategic Defense Initiative (SDI) and Federal programs.

Nomenclature

a	=inner radius of coil, m
b	=outer radius of coil,m
B, B_r	=radial magnetic field,T
C	=capacitance of storage bank, F
E_θ	=azimuthal electric field, V/m
F_z	=axial force, N
g	=acceleration of gravity,m/s^2
H_z	=frequency (1/s)
I_1	=circuit current, A
I_2	=plasma current, A
I_{sp}	=specific impulse,s
j_θ	=plasma current density, A/m^2
j_s	=surface current density, A/m^2

L	=circuit inductance, H
L_e	=external (parasitic) inductance, H
L_i	=initial circuit inductance, H
L_o	=coil inductance unloaded, H
ℓ	=stroke length, m
M	=mutual inductance, H
m	=plasma mass, kg
m_o	=total injected mass,kg
P	=power, W
R	=resistance per square of plasma, Ω
r	=radial coordinate, cm
R_e	=external circuit resistance, Ω
R_m	=magnetic Reynolds number
R_p	=resistance of plasma loop, Ω
t	=time, s
t_o	=time equivalent of δ_o,s
T_e	=electron temperature, eV
U_R	=energy loss to plasma resistance, J
U_p	=work done on plasma, J
v	=plasma velocity, m/s
V_o	=initial capacitor voltage, V
z	=axial coordinate, cm
Z	=axial position of current, m
Z_o	=decoupling distance of plasma, m
ΔI	=impulse per discharge, N s
ΔL	=change in circuit inductance, H
Θ	=azimuthal coordinate, deg
δ	=thickness of current sheet, m
δZ	=depth of initial gas layer, m

δ_o =initial thickness of current sheet, m

η =efficiency of thruster

η_R efficiency, resistance limited

ρ_e =electrical resistivity of plasma ,Ω m

ρ_m =axial mass density, kg/m

2. SUMMARY AND CONCLUSIONS

The Pulsed Inductive Thruster is one of four electric propulsion engines under consideration for space-based, multi-purpose electric orbit transfer vehicles (ETV) that will be needed for deployment and logistic support of SDI and man-in-space activities. The other propulsion candidates are the Ion Engine, the MPD engine and the Thermal Arc engine.

This component technology program has addressed thruster circuit component design (coil, capacitors, propellant injector, single and multiple/synchronized spark gap switches and solid-state diode clamps used to prevent capacitor voltage reversal), plasma probe diagnostics and thrust balance measurements for two of the three thruster designs developed during the program, design of a flight-type capacitor, capacitor pad life testing and demonstration of the system in the clamped discharge mode. A numerical simulation of thruster operation was developed and used to elucidate the effects on efficiency of circuit parameters, plasma conductivity and scale size and to project performance to be expected for a high power large scale thruster.

Capacitor test results indicate very long life is obtainable with modest voltage derating using paper/polypropylene capacitors. Similar life test data by Maxwell Laboratories with all-film, polypropylene, capacitors have demonstrated life in excess of 10^{10} shots at pulse rates above 100 Hz. This type of capacitor is well suited for the PIT.

Development of a successful scheme for high-power, high frequency diode clamping has made it possible to operate a high-Q pulsed circuit without significant capacitor voltage reversal, and hence to extend capacitor life by up to two orders of magnitude.

The propellant injection valve developed for this program used a current-pulse actuated "voice coil" in a permanent magnet to discharge gas from the plenum onto the thruster surface. The required life demonstration of 10^6 cycles was exceeded. However, experience with this injector has indicated that a continuous rotary device may be better suited for this thruster. Acceptable propellant placement was obtained with the gas injection nozzle.

A more uniform and compact gas layer could probably be achieved by extending the injector support pylon to direct the gas more nearly perpendicular to the coil.

Plasma probe diagnostics were helpful in understanding thruster operation. Both current density and magnetic field probes showed the need for testing with a larger vacuum chamber to thruster coil diameter ratio and with a stronger induced electric field to ionize and drive the plasma current. Agreement between thrust balance and magnetic probe impulse measurements was achieved. While the plasma current density probe indicated too high a reading close to the coil, it was very useful in determining current sheet thickness.

It is recommended that further diode-clamped testing be done with a modified version of the Mark III thruster. This would consist of building a smaller coil (3/4 meter instead of 1 meter) having 3/4 turn instead of the present 1 turn. These two changes nearly double the induced electric field for a given voltage, while the smaller coil diameter essentially eliminates tank wall interference.

3. BACKGROUND

The Pulsed Inductive Thruster is similar to other inductive plasma accelerator concepts (References 1 through 4) but differs essentially in the use of a multi-strand flat spiral coil which forces the circuit current density to be uniform over the coil area.

3.1 Advantages of the Concept

An inherent advantage of an inductive device is that electrode erosion, which is always a problem in series-connected discharge devices that carry appreciable current, is entirely avoided. Erosion of insulators through proximity of the hot, dense plasma is also a less severe problem than it is in electrode devices for two reasons: 1) Since the plasma current is induced, and azimuthally symmetrical around the system axis, there are no associated concentrations of power density, plasma density, or radiation density. 2) Radiation loading of the thruster by the plasma is much less severe for the PIT than for small-diameter, steady-state, thrusters since immediately upon breakdown the plasma is driven away from the surface and yields back most of its radiation energy when at a distance such that the thruster subtends much less than a half-sphere of solid angle to it. Consequently only a fraction of the radiated energy, which is a fraction of the total energy deposited in the plasma is received by the thruster. The discharge in a DC device, by contrast, is always in direct proximity to the electrodes, and most frequently surrounded by them to the extent that most of the radiant output together with electrode sheath heating and heat transferred by contact with the thruster is absorbed by the device.

An inherent advantage of pulsed operation is that the performance of the thruster is completely characterized by the properties of a single pulse. Thrust, at a particular I_{sp}, is variable from zero up to the maximum by simply varying the pulse repetition rate; no changes of thruster performance (I_{sp} or efficiency) will accompany this change. This property is especially important in the development phase of the thruster where the limitation in pumping speed of practical vacuum systems results in high background pressures during testing of DC devices. In the past, test results have been seriously distorted by reingestion of background gas into thrusters. Pulsed systems, however, produce their characteristic impulse bits before gas returning from the walls of the vacuum enclosure have time to re-enter the discharge; in single-shot testing the thruster is operating in an effectively perfect vacuum, even with slow pumping speed.

3.2 Problems of Concept

Any pulsed device requires means for energy storage and switching, and also for propellant pulsing in a manner that yields small propellant loss as well as optimal distribution in the thruster at the time of a discharge.

3.2.1 Component Life

The life requirements for all system components are severe. As an example, a nominal mission such as a LEO-GEO cargo transfer, which takes 100 days, requires approximately 10^8 pulses of the PIT operating at 10 Hz. The technology of capacitors, which we use for energy storage in the PIT, has only recently produced life of this order, and that for pulse service less severe than that of PIT Mark I and II operation. (The present program has included capacitor life testing under conditions representative of present requirements; results are presented in section 4 of this report.)

We have employed spark-gap switching for the research thrusters described in this report. On the basis of empirical formulas relating gap erosion to total charge transfer, one may actually design switches for the PIT that should have 10^8 shot life. (The PIT MKII incorporates these.) However, in terms of cooling and gas circulation requirements, as well as erosion, we judge this technology to be unsuitable for an operational thruster. Suitable technologies appear to be near at hand, however; thyristors and thyratrons that are probably combinable into arrays capable of switching the PIT bank are available.

3.2.2 Thruster Mass

A valid comparison of thruster mass can only be made by including power conditioning systems in the calculation. The laboratory PIT thuster is heavy due mainly to the capacitor bank used for energy storage. However, these serve the same function for this thruster as the power conditioner does for a DC arc thruster where electrical power is input at relatively high impedance and delivered to the plasma at low impedance, typically about ten milliohms. Also, capacitor mass must be judged in terms of power rather than energy storage. A ten-fold pulse rate increase reduces the specific mass (kg/kW) by the same factor for a given energy storage mass. A proper comparison of propulsion specific mass including all thruster and power conditioner elements would probably not result in differences for the different electric propulsion candidates that would be significant compared to the power source specific mass.

3.2.3 Propellant Valve

Propellant must be "puffed" into a pulsed thruster by a fast, repetitively operated valve whose lifetime requirement is the same as that of capacitors or switches, i.e., in excess of 10^8 cycles. This is usually regarded as the most difficult of the life requirements because the valve is a mechanical device, and possible material fatigue must be considered.

4. EXPERIMENTAL AND THEORETICAL BACKGROUND

4.1 Experiments

This program is an outgrowth of previous research done at TRW on the Pulsed Inductive Thruster concept. All the thrusters studied in this and earlier programs have employed flat spiral induction coils, with propellant injected from an annular nozzle at the system axis.

Performace achieved with previous thrusters is:

Diameter	ISP	Eff
0.2 m	1200 s	.05
0.3 m	1470 s	.18

A reconsideration of these data, employing the approximate theoretical scaling model given in the next section, led to the conclusion that for the plasma conditions typical of MHD thrusters, there would be a substantial increase in efficiency available through going to a larger coil size. The 1-meter coil size of the thruster used in the present contract is the largest scaleup possible with the available 4 foot diameter vacuum chamber.

4.2 Theory

4.2.1 Elements of the System

The impulsive, inductive acceleration of plasma is conceptually a very simple process as idealized in Fig. 4.1. A strong, short pulse of current is sent through a flat annular coil from a low inductance capacitor bank. A layer of gas, transiently applied to the surface of the coil, is made to break down electrically by the induced azimuthal electric field and the resulting plasma current ring is repelled away from the coil by, as one wishes to view it, a jxB force arising from interaction between the radial magnetic field and the plasma current or by the mutual repulsion of the two oppositely flowing current rings (plasma and coil).

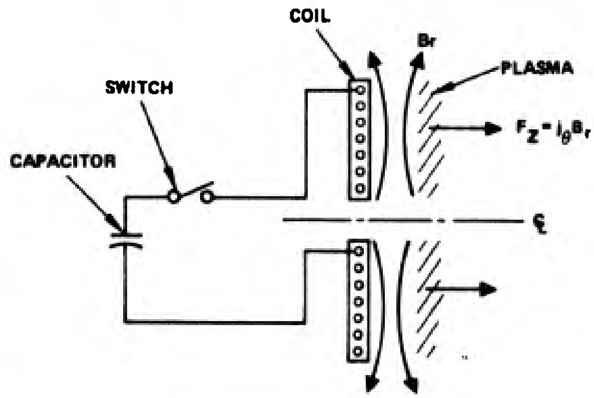

Figure 4.1 Circuit diagram of pulsed inductive accelerator.

Simplicity disappears from the problem, however, when one seeks to maximize the energy efficiency of the accelerator. Motion of the plasma ring away from the coil rapidly decouples the two current rings. System design must provide that most of the stored energy be transferred to plasma motion before this decoupling occurs. Unavoidable energy losses occur in the electrical resistance of the coil circuit and plasma, with the latter being the most serious.

An easily derived theorem shows also that the efficiency of a pulsed accelerator, either inductive or series connected, cannot exceed the fractional increase in driving circuit inductance during the stroke, i.e.,

$$\eta < \Delta L / L_i$$

where L_i is the initial circuit inductance and η the efficiency.[7] Parasitic inductance in the circuit must therefore be rigorously minimized.

Finally, nonpropulsive energy losses occur if the body of plasma is not accelerated uniformly as a rigid body.[8] In the "snowplow" limit where the jxB force is applied to a thin layer at the rear of the plasma, half of the work done by the field goes into the internal, rather than translational, energy of the propellant.

4.2.2 Plasma Resistance Losses and Scaling

When induced electric field E_θ is applied to the propellant gas at the time of circuit switch closure, breakdown follows quickly, i.e., in a time much shorter than the coil current onset time. However, the breakdown interval is not negligibly small, and during this time the conductivity of the plasma swings from zero upward to a value set by the radiatively limited electron temperature. As a result, the initial current sheet thickness in the plasma is somewhat greater than it would be if governed by diffusion at the final T_e.

To simplify discussion of the resistance problem, we consider the one-dimensional situation of Fig. 4.2. Assume that at t=0, the plasma current sheet has a thickness δ_o imparted to it at breakdown. It is accelerated rightward by a constant B and thickens to a δ by classical diffusion as it moves. Acceleration terminates at some distance ℓ from the surface of origin. This represents the decoupling distance for the annular coil accelerator and, since it is proportional to coil diameter, it may be taken as a linear scaling parameter for the system.

For unit current sheet area, resistive power is $P = j_s^2 R$, where $j_s = B/\mu_o$, $R = \rho_e/\delta$, and ρ_e=resistivity.

For classical diffusion

$$\delta = \sqrt{\rho_e t/\mu_0}$$

where t is time since the switch-on of B to the conductor surface. It will be convenient to account for our starting δ_o by shifting the origin of time, so that acceleration starts at

$$t_0 = \mu_0 \delta_0^2/\rho_e$$

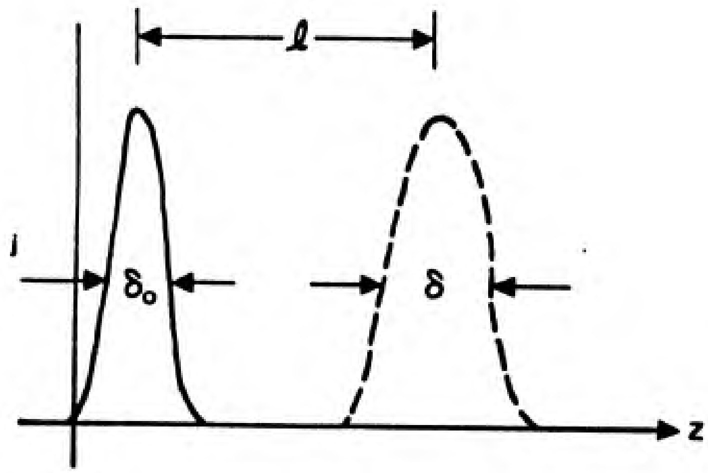

Fig. 4.2 Thickening of resistive current sheet with increasing time.

Then,

$$P = j_s^2 R = \frac{B^2 \rho_e}{\mu_0^2 \delta} = \frac{B^2 \rho_e^{1/2} t^{-1/2}}{\mu_0^{3/2}} \qquad (1)$$

For the case of the heavy-ion plasmas employed for propulsion, it is a convenient and quite accurate approximation to assume that resistivity is constant throughout the cycle. The availability of higher ionization states at higher temperatures, with radiation power dependent on the ionic charge squared, tends to strongly "thermostat" electron temperature, so that for argon, as an example T_e is within half a volt of 3 eV for current densities that differ by more than three orders. Thus we can assume a value of $\rho_e = 10^{-4}$ Ωm for any current densities of interest in this problem. ρ_e is also independent of electron density, except for a weak logarithmic dependence on its square root.

The total resistive energy loss for an acceleration time t is then

$$U_R = \int_{t_0}^{t_0+t} P\,dt = \frac{2B^2 \delta_0}{\mu_0}\left[\left(1+\frac{t}{t_0}\right)^{1/2} - 1\right] \qquad (2)$$

Propulsive work done on the plasma during the stroke of lengh ℓ is

$$U_p = (B^2/2\mu_0)\ell \qquad (3)$$

Also, for constant acceleration, t=2ℓ/v, where v = final velocity. These combine to give

$$\frac{U_R}{U_p} = \frac{4\delta_0}{\ell}\left[\left(1+\frac{t}{t_0}\right)^{1/2} - 1\right] \qquad (4)$$

$$= \frac{4\delta_0}{\ell}\left[\left(1+\frac{2\ell\rho_e}{\mu_0 v\delta_0^2}\right)^{1/2} - 1\right] \qquad (5)$$

The efficiency, as limited only by plasma resistive loss, is then

$$\eta_R = \frac{U_p}{U_p + U_R} = \frac{1}{1+(U_R/U_p)} \qquad (6)$$

The extreme limiting cases of t/t_0 in Eq. (4) are of interest. If $t/t_0 \ll 1$, we obtain, to first order,

$$\frac{U_R}{U_p} = \frac{4\delta_0}{\ell}\left(\frac{t}{2t_0}\right) = \frac{2\rho_e}{\mu_0 v\delta_0} = \frac{2}{R_m} \qquad (7)$$

where R_m is the magnetic Reynolds number of the plasma

Table 1 Effect of scale on thruster efficiency

ℓ, m	t/t_0	η_R
0.05	1.78	0.56
0.10	3.56	0.60
0.20	7.11	0.64
0.50	17.8	0.71

This is the case of a current sheet already so thick at formation that diffusion does not significantly thicken it during the stroke. Plasma velocity or specific impulse is a parameter here, but the scale size of the thruster is not.

For $t/t_0 \gg 1$,

$$\frac{U_R}{U_p} \simeq \frac{4\delta_0}{\ell}\left(\frac{t}{t_0}\right)^{1/2} = 4\sqrt{2}\left(\frac{\rho_e}{\mu_0 v \ell}\right)^{1/2} \qquad (8)$$

In this instance, the current layer thickens significantly during the stroke and the plasma ring resistance drops. ℓ is now a parameter, such that a large accelerator improves efficiency.

Table 1 shows the effect of scale on efficiency for typical thruster parameters: $v=2\times10^4$ m/s, $\delta=0.015$ m, and $\rho=10^{-4}$ Ω m. Here δ_0 and η are values usually achieved in these systems; they are not easily controllable.

While the above analysis is idealized it demonstrates that, *for the plasma parameters achievable in a pulsed inductive accelerator, efficiency, as limited by resistance loss, improves with size of the thruster.*

4.2.3 Numerical Simulation

We have simulated the pulsed inductive accelerator numerically with a model that represents the electrical parameters of the system quite accurately, but uses a highly idealized and approximate model of the plasma.[9]

Electrically, the thruster is modeled as a transformer of one turn in both primary and secondary. The primary is driven by a capacitor C, charged to voltage V_0; it contains parasitic inductance L_e and resistance R_e. The plasma secondary has resistance R_p. Figure 4.3 is an equivalent circuit of the system.

Both the coil and plasma are flat annuli of outer radius b and inner radius a. Each has inductance L_0 and they have a mutual inductance M(Z), where Z is the axial separation between the two loops.

To within a few percent, the inductance L_0 is given by

$$L_0 = \mu_0 \frac{(a+b)}{2} \left[\ln \frac{b+a}{b-a} + 0.9 \right] \qquad (9)$$

and, empirically, we find that the mutual inductance is well approximated by

$$M = L_0 \exp(-Z/2Z_0) \qquad (10)$$

If the primary and secondary currents are designated I_1 and I_2, an easily derived relation gives the force of repulsion between these currents

$$F_z = -I_1 I_2 \frac{\partial M}{\partial Z} = \frac{I_1 I_2 L_0}{2Z_0} \exp(-Z/2Z_0) \qquad (11)$$

Then Newton's law couples the electrical and mechanical systems

$$\frac{d}{dt}\left(m \frac{dZ}{dt}\right) = \frac{I_1 I_2 L_0}{2Z_0} \exp(-Z/2Z_0) \qquad (12)$$

The simplest representation of the plasma is that of a thin sheet of fixed mass m and assigned resistance R_p. We may use

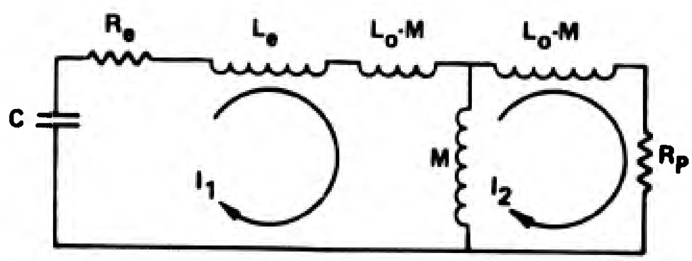

Fig 4.3 Accelerator equivalent circuit

it to solve the coupled electromechanical equations and obtain a plasma trajectory and accelerator energy efficiency. Such a grossly simplified model is not very useful, however, because it neglects the two important effects mentioned earlier as being major determinants of efficiency, i.e., the variable plasma loop resistance and "snowplow" losses associated with nonuniform acceleration of the total mass.

Accordingly, we have adopted a plasma model that incorporates both of these effects. We assume:

1) The total injected mass m_0 is distributed uniformly over the annular coil in a layer of thickness δZ. While the current sheet moves outward through this interval, the total force on it is

$$F_z = \rho_m \left[Z \frac{d^2Z}{dt^2} + \left(\frac{dZ}{dt} \right)^2 \right] \quad (13)$$

while, for $Z > \delta Z$

$$F_z = m_0 \frac{d^2Z}{dt^2} \quad (14)$$

and we have passed from initial snowplow acceleration to slug model acceleration. In Eq. (13), $\rho_m = m_0/\delta Z$ is the initial axial gas density (in Kg/m).

2) At t = 0, we must assume a finite plasma mass as well as an initial current thickness δ_0. For simplicity, we start with $m = \rho_m \delta_0$, where δ_0 is arbitrarily assigned (we rely on experimental experience for approximate values). Plasma loop resistance is then

$$R_p = \frac{\pi(b+a)}{(b-a)} \left(\frac{\rho_e}{\delta} \right) \quad (15)$$

where, as shown earlier,

$$\delta = \sqrt{\frac{\mu_0 \rho_e}{t + t_0}}$$

and

$$t_0 = \mu_0 \rho_e / \delta_0^2$$

This model was used for initial estimates of attainable efficiency as a function of scale size of the thrusters. Initial results were encouraging in two respects. First, the efficiency actually attained in two earlier experiments with 8 and 12 in. coils was in fairly good agreement with the computation. Second, the computation predicted a substantial improvement in efficiency with size, indicating that one might expect an efficiency of 60% for a 2 m coil and 5000s I_{sp}. We were thus encouraged to build the 1 m thruster used in this program.

5. PARAMETERS OF PIT MARK I TO MARK III

The thrusters investigated in the present program have the following parameters in common:

5.1 Coil

The induction coil is a 1-meter diameter flat spiral of one turn. It consists of 36 one-turn spirals of flat "Litz wire" separated from each other by 10 degrees in azimuth and driven in parallel. Each strand of the coil begins at .2 m radius and ends at .5 m; at the outer radius each strand folds radially inward and joins its inner end to connect to one of 36 coaxial cable feed lines from the switch. The resulting current density is purely azimuthal and uniform over the coil. An exception is the outer 6 cm radius, where the pitch of the spirals is decreased so as to double the current density. This compensates for the loss of magnetic pressure which would normally occur at the coil edge due to field fringing.

The coil is embedded in epoxy, with a 1.5 mm layer of Lucite insulation between the conductors and the front surface. An additional 3 mm protective sheet of glass then covers the plastic.

Unloaded inductance of the coil is measured to be 0.70 microhenries, with parasitic inductance of capacitors, conductors, and switch system amounting to 60 to 80 nanohenries, depending upon the particular version of the thruster. The decoupling distance Z_0 (Eq. 10) is 12 cm, as determined by an experiment in which the thruster ringing frequency was measured as a function of the separation distance of an aluminum loading plate. Total circuit resistance was also determined, by the observed damping coefficient in this same experiment, to be 7 milliohms.

5.2 Capacitor Bank

Capacitance of the energy storage banks in MKI and MKII is 20 microfarads; that in MKIII is 16 microfarads. Capacitors in all cases are rated by the manufacturer for 25 kV. Thus, a stored energy of 6.2 kilojoules can be delivered per shot.

5.3 Propellant Increment

The nominal propellant mass injected per shot is 10^{-5} kg, although this figure is variable, depending upon the value of I_{sp} desired.

5.4 Impulse, Thrust, Power

If one assumes that a charge energy of 4 kilojoules (20 kV) is imparted to 10^{-5} kilograms of gas at 0.35 efficiency, the resulting impulse bit is 0.167 Newton-second, and the I_{sp} is 1710 seconds. Thus, a repetition rate of 10 hertz would require 40 kW and produce a thrust of 1.67 N, or 0.38 pounds. At 50 Hz, the power would be 200 kW with 1.9 pounds thrust.

5.5 Thruster Mass

The PIT, in its present laboratory embodiment, has a mass of slightly over 200 kg. No special effort has been made to lighten the structure or components.

A rough estimate of specific mass for a flightweight version, operating at 10 Hz has given a value of 1.1 kg/kW[6]. At 50 Hz this becomes 0.44 kg/kW. These preliminary values illustrate the importance of pulse rate for this thruster but should not be regarded as indicative of a propulsion device until a more complete analysis has been made.

6. PROPELLANT SYSTEM

6.1 Requirements and Energetics

Efficient mass utilization, which is necessary for maximum thrust efficiency and I_{sp}, can only be achieved if the gas injection system is capable of covering the coil with a puff of propellant that has not been preceded by gas that has escaped at the time of the shot, and is not followed by any trailing gas that arrives after the shot. This requires that the valve be fully opened in a time of a few hundred microseconds at most, and be capable of closure in the same time. An equally important requirement is that the valve not consume an amount of energy per shot that is comparable to that used for acceleration, or even sufficient to cause significant heating of the valve at nominal repetition rates.

6.2 Design

Electromechanical valves are invariably driven by magnetic forces. Two general categories of drive may be defined, i.e., self-field drive, in which the applied current interacts with magnetic fields that it has generated, and fixed-field drive in which the current crosses an independently applied field in order to develop force. Eddy-current valves, in which flux from a pulsed coil presses against a highly conducting plate, are examples of the first group. These can be made extremely fast; however, they are usually not efficient because the developed force varies as the square of the current, so that charge flowing from the storage bank at much less than the peak current does little useful work.

We have therefore opted for the second category. The valve has the physical configuration of a large loudspeaker driver, in which an externally driven "voicecoil" is positioned in the annular gap of a strong permanent magnet (Fig. 6.1). In the present case, the coil form is 6 cm diameter, 3 cm long, 1 mm thick cylinder of alumina into which grooves for 25 turns of #20 wire have been ground. It is brazed to a taut stainless steel diaphragm of .05 mm thickness which serves to position it accurately in the 3mm magnet gap, and also to provide a barrier between the gas-filled coil region and the vacuum of the exit nozzle throat and the propellant plenum.

The backside of the diaphragm is contacted by an O-ring of 6 cm diameter that separates the central plenum region from the radially symmetrical nozzle throat. Seating force for the valve seal is provided by the difference of integrated gas pressure on the two sides of the diaphragm; diaphragm tension itself is relatively small at nominal values of displacement.
The permanent magnet material is Cerium-Cobalt, producing in the annular coil gap a field strength of 1 Tesla.

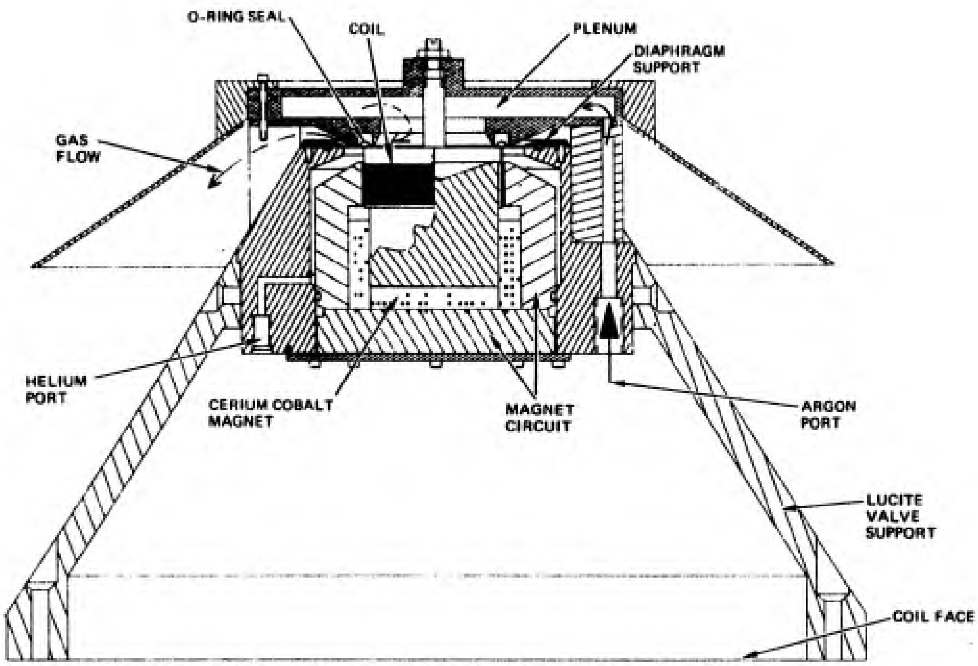

Fig. 6.1 Gas injection valve cross section

6.3 Electrical Design

The initial electrical design concept took advantage of the fact that a fixed-field electromagnetic driver is bidirectional; i.e., a reversal of current results in a reversal of force. (This contrasts with self-field devices that are capable of developing force in only one direction.) In this scheme, the large forces that are necessary to open the valve and to close it again in a very short time are both produced by the applied current; the diaphragm and the differential gas pressures are thus not required to supply large mechanical forces.

Drive energy is stored in capacitors and switched with thyristors. The original arrangement provided four successive drive impulses that, in order : 1) accelerate the coil and diaphragm to full opening velocity, 2) decelerate to rest at full open position, 3) accelerate toward closure, and 4) bring the mass to rest at closure. (The last deceleration was in order to avoid bouncing and consequent loss of additional propellant at the end of the operation.)

Electrical and mechanical parameters of the system are:

Moving mass	20 g
Capacitance	50 microfarads (per module)
Inductance	10 microhenrys " "
Voltage	300 volts
Acceleration	9×10^5 m/s^2 (9200 g)
Time to open	150 microseconds
Energy	2.3 Joules

Full opening is a gap of 0.5 mm around the 19 cm circumference of the valve seat. Fig. 6.2 is a graph of capacitor voltage, coil current and valve displacement for the first two current pulses, generated by a computer simulation of the system. (The second current pulse and voltage are negative, while drawn as positive on the graph.) Experimental measurement of V and I gave curves nearly identical to these, and measurements of gas flow (described below) indicated approximate agreement with the predicted displacement.

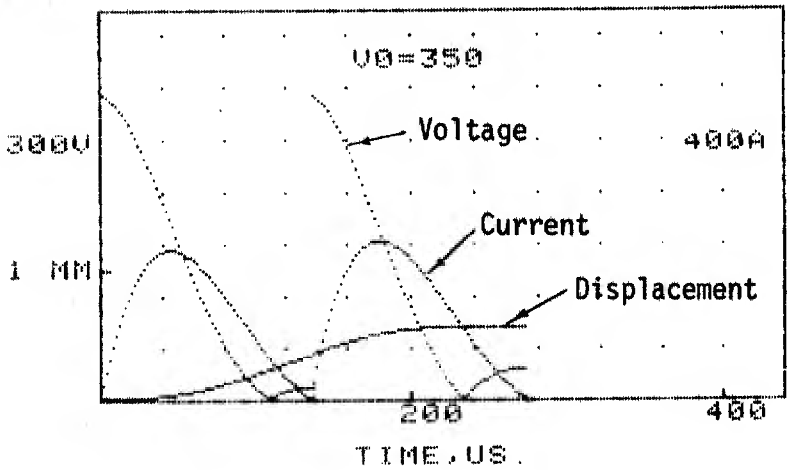

Figure 6.2 Valve Capacitor Voltage, Coil Current and Displacement ($R=0.8\ \Omega$, $L=30\ \mu H$, $C=50\ \mu F$)

It has been found, in actual operation of the valve, that the full speed given by the above parameters is not necessary for attainment of an optimum propellant distribution on the coil. In particular, we have determined that one atmosphere of pressure on the coil side of the diaphragm provides an adequate net return force when the propellant plenum pressure is itself one atmosphere. A single capacitor discharge (150 volts, 200 microfarads) meters a mass increment of approximately 10^{-5} kg, over a flow time of about 500 microseconds. Thus, the entire energy consumption per shot is 2.3 joules. Experiments conducted during this program have not involved sustained high repetition rates, so cooling of the valve has not been a problem. However, in the event of rates higher than a few tens of hertz, it will be necessary to remove a hundred watts or more of thermal power from the coil. In this instance, we assume the use of helium as the pressurant in the coil chamber; its low thermal impedance, especially over the narrow gap between the coil and the magnet poles, should maintain a negligible temperature difference between the coil and the magnet frame.

6.4 Gas Supply System

Fig. 6.3 is a schematic of the propellant supply system. The principal function of this arrangement is to provide an accurately controllable and measurable mass increment for singleshot operation. Components are: high pressure supply tank S, plenum-pressure reservoir V_s, calibration volume V_c, plenum volume V_p, manometer M, electronic pressure transducer PT, and valves X_1-X_5.

With X_3 closed and X_1, X_2, and X_4 open, the system is initially evacuated through X_5. Then X_4 and X_5 are closed, and the reservoir V_5 is filled from S to the desired plenum pressure, typically one atmosphere absolute. Just prior to a shot, X_1 is closed; the mass released from V_p (and the plumbing volume associated with it) results in a pressure drop which is read out either on manometer M, or on transducer PT, whose output is A/D converted and read out at the controller terminal as a mass value. In practice, M is used only to calibrate PT.

If the actual value of V_p were known, its pressure drop could be converted directly into mass; however, since it includes several meters of tubing in addition to valves and connectors, such a determination cannot be done geometrically. It is easily accomplished, however, by the addition of an additional and accurately measured calibration volume V_c. It is only necessary to record pressure drops with and without V_c included in order to solve for V_p, and thus to obtain a good determination of the proportionality between pressure drop and mass.

The same system could be used to determine the mass flow rate in repetitive running of the thruster. In this case, X_1 would be replaced by a choke, such that pressure drop across it would correspond to flow rate. (The relation is not linear, but easily calibrated, and could be included in the software that processes the output of PT.)

6.5 Nozzle and Baffle

The valve assembly is mounted on a conical Lucite pylon such that the gas exits radially 23 cm above the coil surface. A conical aluminum "hat", mounted on the top surface of the valve body then deflects the gas flow downward toward the coil at about a 45 degree angle. The cone and the conical pylon surface comprise, in effect, an annular supersonic nozzle. A second conical baffle, not shown in Fig. 6.1, has been placed inside the main nozzle in order to optimize the final gas distribution.

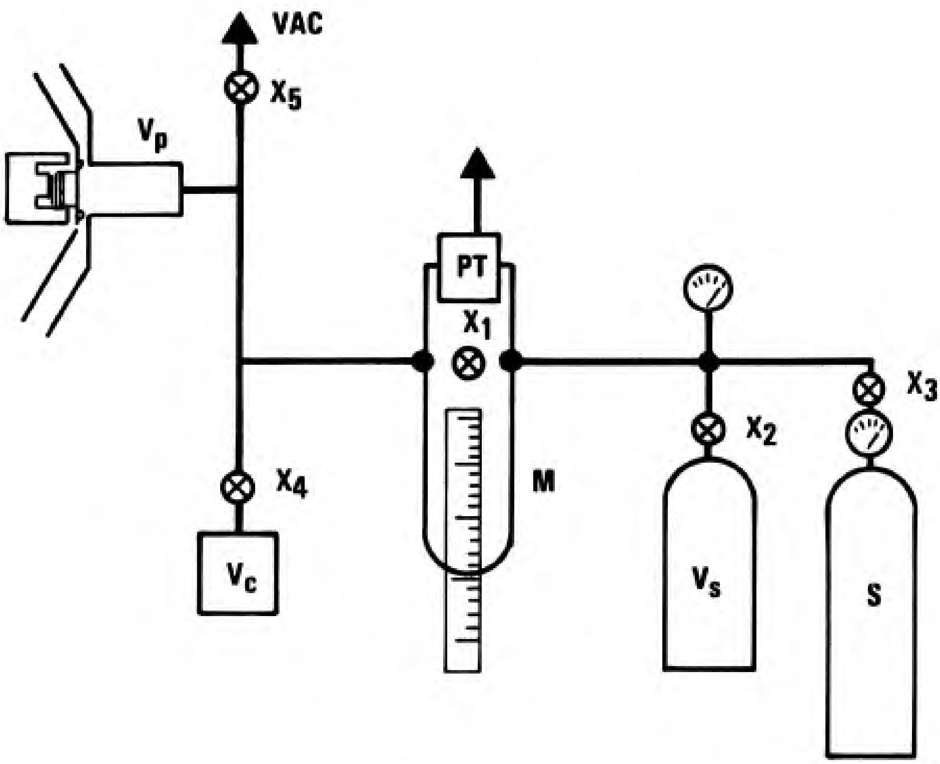

Fig. 6.3 Propellant Supply System Schematic

A 10 cm high barrier, cemented together from flat glass plates, is positioned at the outer radius of the coil, and attached directly to the glass surface insulator. Its function is to deflect the initial toe of the radially advancing gas flow back toward the center, and prevent propellant loss before the tail of the injected mass reaches the coil.

6.6 Propellant Distribution

The success of this thruster concept depends on the achievement of a thin, uniform distribution of mass on the coil at the time of firing. It is, accordingly, essential that there be means for measurement of this distribution, notwithstanding the fact that it is transient in nature.

6.6.1 Fast Ionization Gauge

We have been able to employ a technique developed nearly three decades ago by J. Marshall at Los Alamos (10), in which a small pentode vacuum tube, its glass envelope removed, is used as a fast-response ionization gage. In this application, the screen and suppressor grids are tied together and operated at about 100 volts positive potential, while the plate serves as the ion collector, at ground potential. Strong degenerative feedback between cathode and control grid assures a constant electron current. As in a conventional ionization gauge, the electrons, in oscillating back and forth through the positive grids prior to their capture , collisionally ionize background neutrals, which are then driven to the plate by the potential gradient. The Raytheon CK5702 tube employed here is extremely small, and accordingly, able to function at relatively high pressures before being disabled by breakdown or self-shielding by the plasma it creates. It appears to retain fair linearity up to a pressure of several hundred millitorr. Absolute calibration of the gauge has been done by closing the main tank pump, and injecting into the tank a measured quantity of gas that produces a pressure step of the order of a hundred millitorr; the gauge exhibits a corresponding step, with only a slow sag due to cathode cooling.

6.6.2 Distribution Measurements

Distribution of the gas as a function of position and time was determined by using the fast gauge as a movable probe. Records of pressure as a function of time after valve firing were made over a 60-point grid in the R-Z plane; each record from the digital transient recorder was stored to disk in the system computer, where they were subsequently analyzed. The most useful of the processing routines produces contour maps of pressure at selected times. Examples of these contour maps are presented in Figures 6.4 and 6.5.

Figure 6.4 is for a single-cone nozzle, and four times (1.4, 1.5, 1.6, and 1.7 ms) after switching of the valve current pulse. It may be seen that the gas pulse is very compact, corresponding to a total open time of the valve of 400 microseconds; in fact, it is too compact for optimum distribution over the coil. Included on each plot is the result of integration of the distribution over space, expressed as a total mass. It is seen that over this time interval, conservation of the gas is excellent.

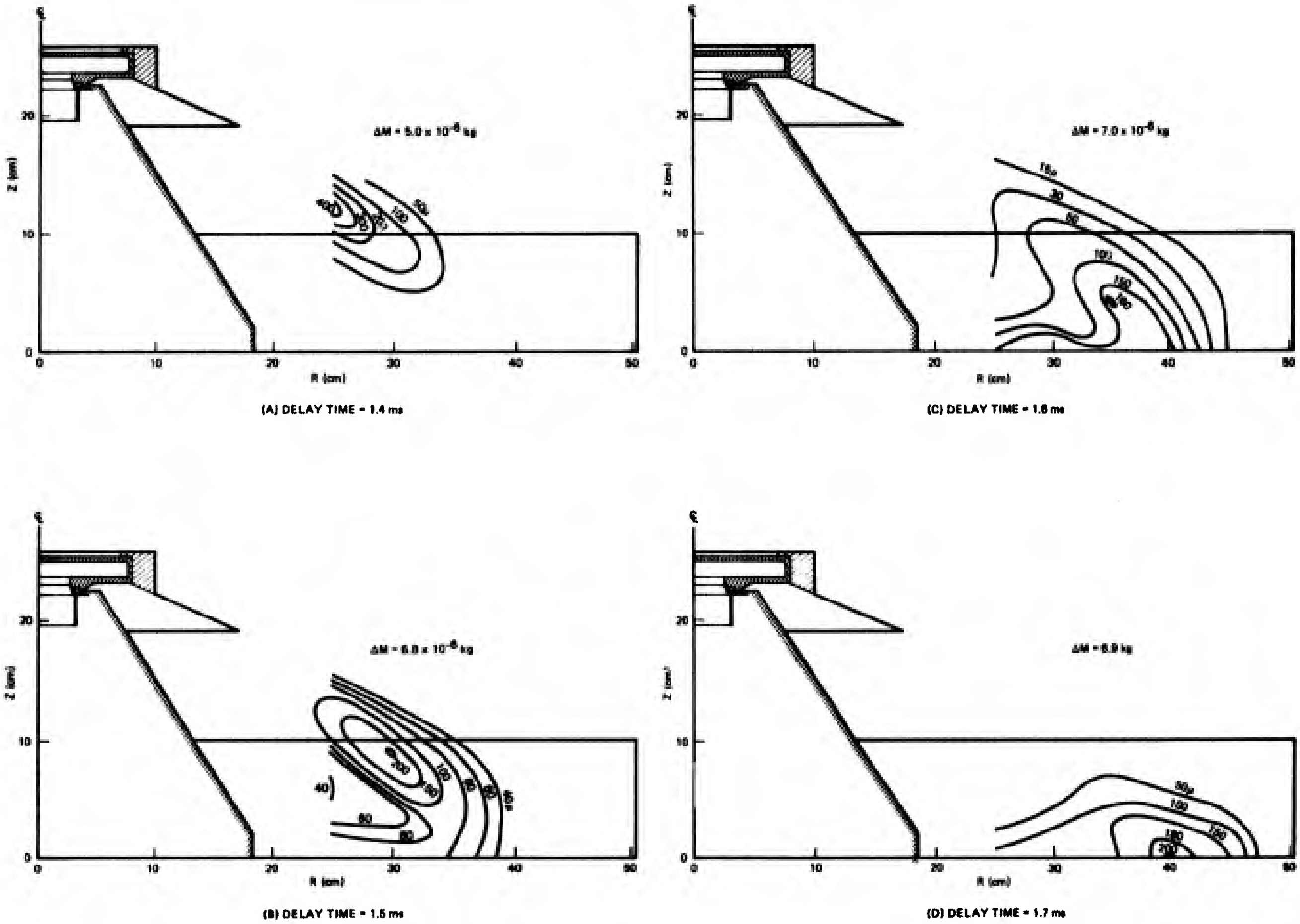

Figure 6.4 Constant density contours for single cone nozzle

Figure 6.5 is for the case of a dual-cone nozzle. Here, about half of the gas has been directed sharply downward by the inner cone toward the 20-30 cm radius zone of the coil. As it flows outward along the surface, that portion deflected by the outer cone reaches the surface, and provides enough normal momentum flux to prevent premature outward expansion of the layer. This particular distribution is as close to ideal as any achieved in this program.

6.7 Valve Life Test

Early attempts to demonstrate 10^6 cycles valve life encountered a problem with lead wire attachment to the coil wire. This was overcome by soldering beryllium-copper leads to the copper wire valve coil. With this technique a life of more than 2×10^6 cycles was demonstrated. The test was terminated by rupture of a current return wire that had not been secured with epoxy.

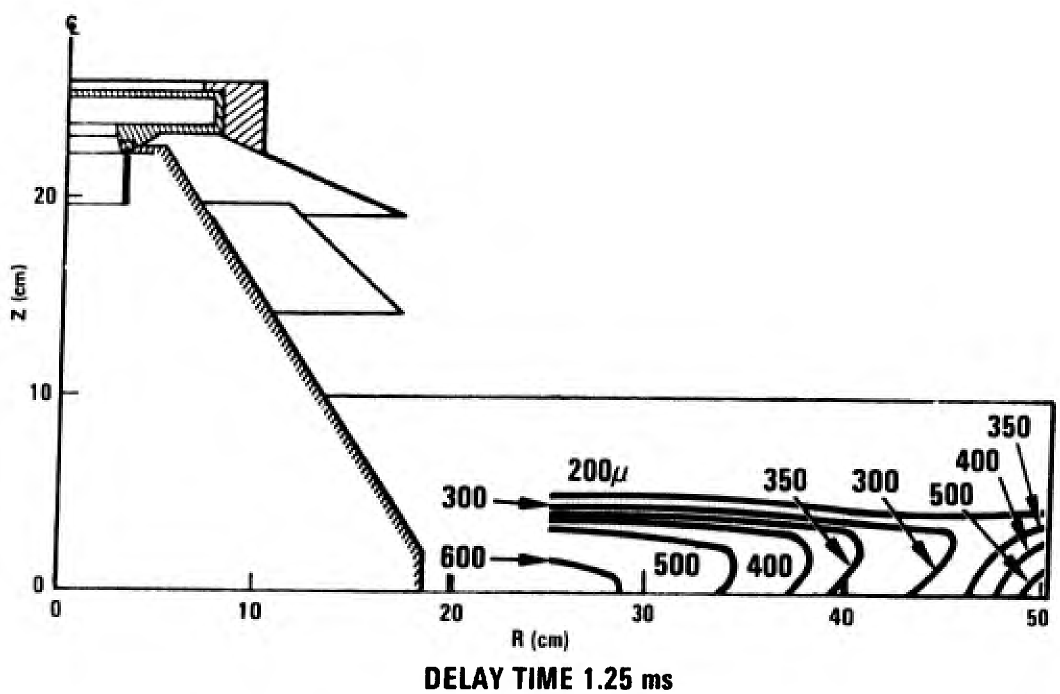

Figure 6.5 Constant density contours for dual-cone nozzle

7. CAPACITORS

7.1 Selection Criteria

The criteria which must be met by capacitors used for energy storage in a pulsed thruster are those generally regarded as important for many other applications: i.e., acceptable energy density, low dissipative loss, and long shot life. The order of importance of these criteria will differ from one application to another, however, and this ordering will make a major difference in the selection of an optimum technology.

For thruster application, lifetime outweighs all other considerations. The loss factor is clearly of importance, since thermal losses result in lowered thruster efficiency, and the heat must ultimately be rejected radiatively by the spacecraft. Moreover, there is usually a negative correlation between dielectric losses and lifetime. Excessive capacitor mass is obviously undesirable, since it raises the specific mass of the overall power system and, for all other things equal, decreases the deliverable payload fraction for a given mission. Nevertheless, while reasonable heat loss and capacitor mass can be accomodated and compensated for (e.g., by repetition rate), capacitor failure cannot. The consequences of capacitor failure can be somewhat mitigated, as in the Mark II design, by subdivision of the bank and switching system so that a failed module can be disconnected with minor effect on performance of the remainder.

As an example of an otherwise impressive technology whose selection for a thruster would be inappropriate, one may cite the use of "K-film" dielectric. Its attainable energy density is very high (100 J/kg), making possible an unusually light storage bank; however, its dissipation factor is also high, and the film itself is extremely heat-sensitive. The result is a tendency toward failure at high pulse rate so that the use of increased repetition rate to reduce capacitor mass at a given power is not possible.

Of equal importance to the choice of capacitor technology (dielectric and impregnant) is the selection of a range of operating parameters, i.e., dielectric stress E, total voltage per pad V, and voltage reversal. An empirical formula for lifetime as a function of these parameters that has been used in the capacitor industry (11) is:

$$L = \text{const} \times E^{-3.5}\ V^{-4}\ Q^{-1.6}$$

where Q has its usual definition for an oscillating circuit. This equation contains the interesting result that field strength in the dielectric and overall voltage have separate effects. The appearance of corona tracks at foil edges and the frequent failures at these points may be attributed to V, for example.

7.2 PIT Capacitor Technology

Capacitors used for the PIT employ a polypropylene and paper dielectric. The paper, interleaved between layers of plastic film and the foil electrodes, serves as a wick that ensures complete penetration of the oil impregnant to all regions of the capacitor. The loss factor of this dielectric (0.001) is nearly all attributable to the paper. Recently developed all - polypropylene capacitors have exhibited loss factors sufficiently low as to allow pulse repetition rates of over 100 hertz and lifetimes of 10^{10} shots, while operating at energy densities comparable to those employed for this thruster. Pulse rates as high as 1 kHz have been used in energy discharge tests with this capacitor.

7.3 Voltage Reversal

The quantitative dependence of capacitor lifetime upon the degree of voltage reversal during a discharge has been a subject of considerable disagreement, notwithstanding the proposal of such relationships as that given in section 7.1. Nevertheless, there is general agreement that reversal is deleterious to capacitor life.

When actual comparisons of lifetime for critically damped wave forms and for 50% reversal were obtained in the present test program, it became clear that an extremely severe penalty in lifetime is associated with the amount of voltage reversal produced by the PIT. At this point, a decision was made to attempt to clamp the capacitor bank against reversal.

7.4 Diode Clamping

A widely used method of avoiding capacitor reversal in pulsed systems is to "crowbar" the inductive load with a second spark gap switch placed directly across the load terminal and fired at approximately the first voltage zero (or current peak). While this procedure could, in principle, be used here it adds to the thruster another entire switching system, together with rather severe requirements for its timing.

A second and much simpler method is to place a diode clamp across the circuit, such that it conducts when the load voltage reverses. Like the crowbar switch, it would then prevent the return flow of energy into the capacitor, and thus prevent voltage reversal. The load itself would, after the clamping, be subject to a monotonic driving current which should result in better efficiency than is attainable from an oscillating current.

Use of diode clamping for fast pulsed systems such as the PIT has not, however, been seriously considered because of the severe requirements, e.g., $\sim$100 kA peak current, 25 kV reverse voltage, and turn-on time of a small fraction of a microsecond. However, considering the rapid rate of development of high-power solid state components, an experimental survey of presently available diodes was made to determine if some reasonable array of them might meet the needs of this application.

The typical specifications for a diode include its peak inverse voltage, average forward current and maximum surge current, the latter usually specified for a particular duration, e.g., one-half of a line voltage cycle. This limit appears actually to be set by the pulsed thermal energy it takes to destroy the junction; accordingly, some specifications include an upper limit on the product $I^2\Delta t$. It is implied by this that the allowable surge current should scale about as $(\Delta t)^{-1/2}$, from which one concludes that the half-cycle surge value might be safely exceeded by a factor of nearly 30 if the current pulse is 10 microseconds long.

The first test of diode clamping was done in the capacitor test apparatus with a standard 1.3 μFd pad connected to an RL circuit that produced 50% reversal with a 23 μsec period. A Semtech SCH25000 high voltage (25 kV) rectifier, rated at 0.5 ampere average current and 50 ampere half-cycle surge was placed across the circuit at the load terminals. At a charge voltage of 6 kV, it produced excellent clamping, but failed at 7 kV. Its peak current at failure was about 1200 amperes, a factor of 24 above rated surge, which agrees quite well with the thermal failure hypothesis. A second test with a unit (SCHS15000) rated at 150 amperes surge produced failure at 4500 amperes (pulse peak), again an excellent agreement with $(\Lambda_t)^{-1/2}$ scaling.

Accordingly, the capacitor test apparatus was modified to include a parallel array of six SCHS15000 diodes as clamps. For nearly all of the test data that approximate thruster conditions (6 - 7 kV/pad), a single diode would survive isolated shots; however, in order to accumulate data fast enough to get life data in practical times, it was desirable to use a pulse frequency of at least 20 hertz. The six parallel units were necessary in order to hold the temperature rise of the diodes to a safe value at 20 Hz frequency and using available forced-air cooling.

In order to discuss and analyze properly the currents and voltages in a clamped discharge circuit, we employ the network shown in Figure 7.1

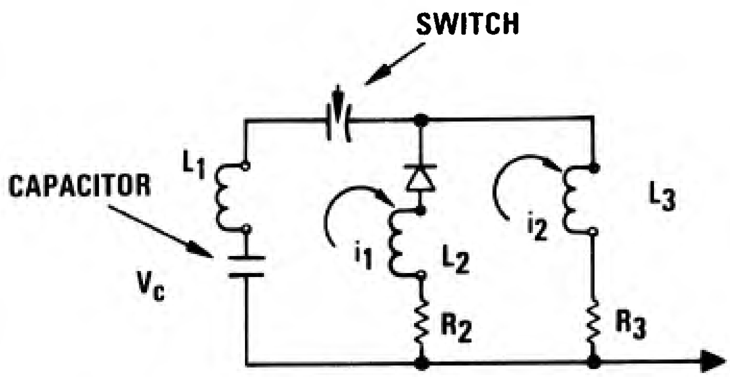

Figure 7.1 Clamped Discharge Circuit Network

Typical waveforms for currents i_1 and i_2, and capacitor voltage V_c are represented in Figure 7.2. It can be seen that up until the clamp time t_c, i_1 and i_2 are the same, and have a period τ_1, determined mainly by C and the load inductance L_3. After t_c, however, i_1 oscillates at a much higher frequency and lower energy, and i_2 decays exponentially. The slight oscillation in i_2 just after t_c is due to the residual coupling between the otherwise isolated circuits provided by L_2 and R_2. The important advantages

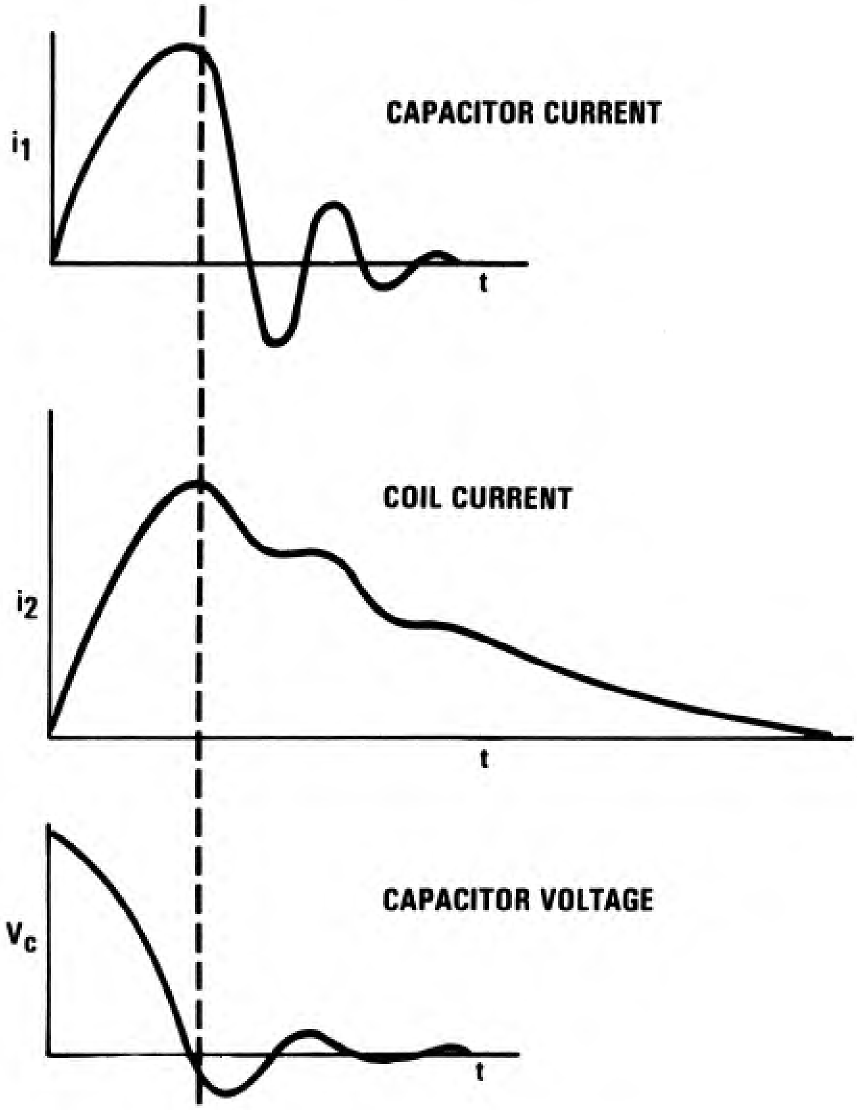

Figure 7.2 Clamped Circuit Currents and Voltage

of this scheme are (1) that the reversal in V_c subsequent to t_c is quite small, and (2) nearly all of the original stored energy is now locked into the load inductance. In the circuit of Figure 7.1, it would decay into heat in R_3, but in an accelerator this field energy is released as well by expansion work against the plasma.

7.5 Computer Thruster Circuit Simulation

We have written a computer simulation of the circuit of Figure 7.1, including the time-varying inductance associated with actual mass acceleration of the plasma, and also coupling with the circuit equation the momentum equation of the mass itself. The result of a run made with our best estimates of the actual circuit parameters is given in Figure 7.3. The circuit inductances are actual measured values (L3 is the beginning inductance of the load), and resistances are inferred from dummy-load tests and earlier plasma data on the Mark I thruster. (These values are all for Mark II.)

The significant results of this run are that the current waveform is a quite accurate approximation to those actually observed in Mark I, both in the magnitude (120 kA) and time (2 μs) of the first current peak, and also the time of the first voltage zero, where I_1 breaks downward. (On previous thruster data, I_1 broke downward at the voltage zero point, due to the slight clamping effect of the formation of a new current sheet at the coil surface.) The diode clamp is thus delayed well beyond the current maximum in going into conduction. The maximum current required of the diodes, equal to the difference between I_2 and I_1 is thus only about half of the 120 kA total current peak.

More importantly, the substantial phase lag in the voltage zero time has the effect of reducing the voltage reversal; here it is only about 10%, thus the clamped capacitor life can be expected to lie between the non-reversed and diode clamped values.

7.6 Test Results

The dielectric combination selected for the Mark II capacitor design consisted of 3 layers of 0.3 mil paper and 2 layers of 0.433 mil polypropylene film arranged with paper against the aluminum foil (0.25 mil) and between the film layers. The active dielectric length was 2.88 inches and edge margins were 0.625 inch. Each pad consisted of two series wound sections

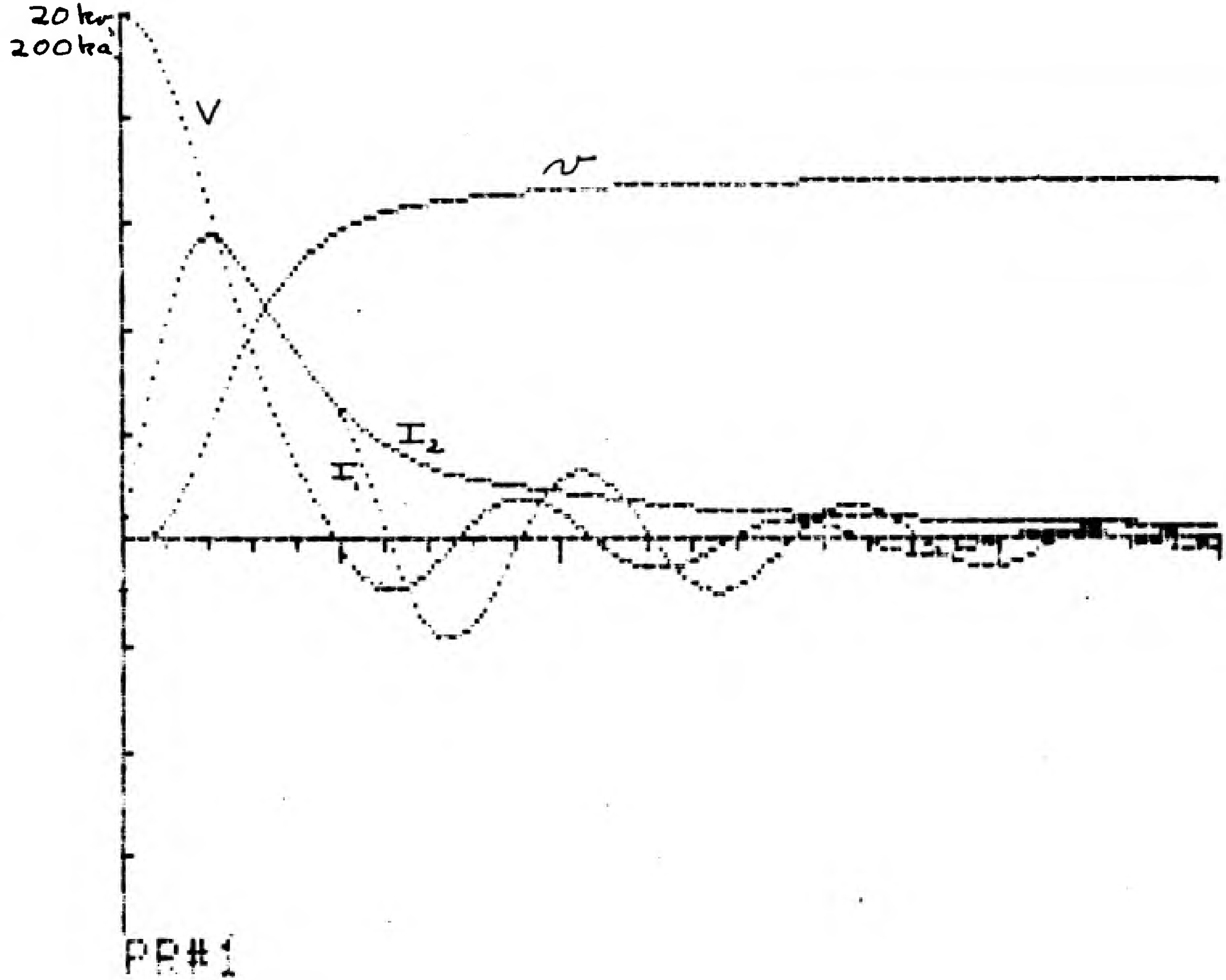

Figure 7.3 Computer Simulated Thruster Characteristics

having a 1 inch gap separating the sections at the center of the winding. Four of these double pads were connected in parallel and then connected in series with another parallel assembly of four double pads. A total of 25, steel encased, 1.67 μF capacitors were built. Twelve were later modified by removing some of the pads to make room for the diode strings that served as clamps across the capacitors to prevent 2nd half-cycle recharging. Actually 13 capacitors were used to get 12 successful modified units. The modified capacitance was 1.3 μF.

To obtain life data on this design, 50 individual pads (not series wound) were separately encapsulated in plastic cases. These pads were identical with those in the flight type units except that the edge margins were increased to 1.25 inches to allow testing to a hi-pot failure without flash-over.

Life test results are plotted in Figure 7.4 for the 50 pads. As indicated in the figure, three test modes were used: 1) Ringing discharge with 50% voltage reversal, simulating Mark I and Mark II operation, 2) Critical Damping (no reversal) and 3) Diode clamped discharge simulating Mark III operation. Also shown in the figure are comments suggesting interpretation of failure modes. These are not based on post mortem examinations but are suggested by the shape of the life curves.

For the critically damped condition, there seems to be three regimes. At high voltage, 14 to 16 kV, the curve is very steep suggesting edge margin flash-over. This seems likely in that the design was based on a nominal life of 10^8 shots at 6.25 kV. The test pad edge margin was twice that of the flight capacitors to permit failure testing well above design voltage. It appears from the data that the edges were satisfactory up to 13 kV, i.e., twice the nominal capacitor design voltage.

In the range of 9 to 10 kV, the life curve slope is much lower than at lower voltages, suggesting a more rapid wear-out mechanism such as corona erosion. Below 9 kV the curves for both the critically damped and diode clamped discharges are very steep. In fact testing was terminated without failures at the lowest voltages (6 kV for the diode clamped mode and 7 kV for the critically damped discharge).

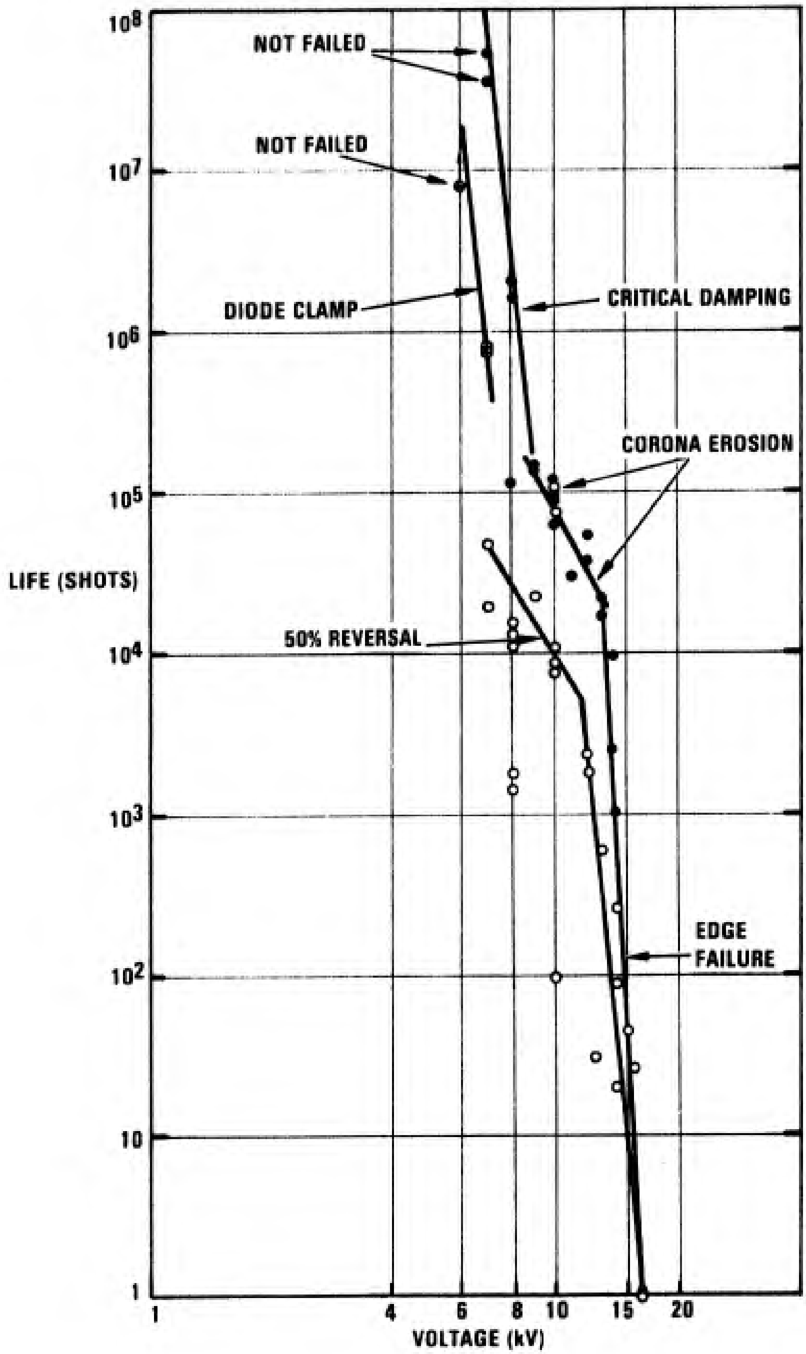

Figure 7.4 Capacitor Pad Life Test Data

We, and others in the energy discharge business, have suspected for a long time that at voltages sufficiently low, capacitors should be capable of an unlimited number of discharges in much the same way that metal fatigue disappears below some stress level. This is suggested for capacitors by AC capacitors and by automobile engine ignition capacitors. This is not conclusively demonstrated by the limited Figure 7.4 data, but it is strongly suggested.

During the past 2 years, after the present capacitors were built, Maxwell Laboratories has achieved very long life data with all-film, polypropylene, capacitors. It appears now that these capacitors are capable of a few times 10^{10} discharges at a pulse rate of 1 k Hz.

If the life curve slope is really as steep as indicated in Figure 7.1, for long life operation, a factor of 10 increase in thruster operation life can be obtained with very little capacitor voltage derating. For the present data

$$\frac{N_2}{N_1} = \left(\frac{V_2}{V_1}\right)^{-25}$$

If we decide to increase shot life from 10^{10} to 10^{11}, the associated voltage derating ratio is

$$\frac{V_2}{V_1} = \left(\frac{N_2}{N_1}\right)^{-\frac{1}{25}} = 0.91$$

which reduces the power by 0.83. The power is restored to the original value by increasing the pulse rate by 1/.83=1.20. If the original life of 10^{10} shots was accumulated by operating the thruster 3.2 years at 100 Hz, a voltage derating of 0.91 would allow the thruster to operate at the same power by increasing the pulse rate to 120 Hz for (10/1.20) (3.2) = 26.7 years. In other words, essentially unlimited energy discharge capacitor life can be achieved by derating. As an example, Maxwell has obtained 2.2×10^{10} shots at an energy density of 6.6 joules/lb. This life corresponds to 70 Hz for 10 years. The corresponding specific mass is 10^{-3} kg/kW.

It is concluded that all-film, polypropylene, energy discharge capacitors do not impose a mass constraint, a life constraint or a pulse rate constraint on thruster design.

7.7 Thruster Diode Clamp

Clamping of the full thruster bank is not feasible with diodes as small as the Semtech units used for individual pad testing; the required array would be impractically bulky and expensive. The diode module that was found to be suitable for the thruster in reasonable numbers is the Westinghouse R620. It is physically a small disk, 0.5" x 1.5" which has a peak inverse voltage rating of 2600 V and a forward half-cycle surge rating of 5000 amperes. They were clamped together in stacks of ten, with one stack clamping each of the 12 1.67 μF capacitors.

Initially, a test of one stack connected across the input of an RL load in the capacitor test stand and driven by one of the capacitor-switch modules from the thruster, produced excellent clamping up to 25 kv charge voltage. However, when the entire bank of diode-clamped capacitors was fired into the dummy-loaded thruster coil, a majority of the diode strings failed within the first three shots. It was ascertained that this failure resulted from a reflection of a double-voltage transient backward to the diodes from the far end of the coaxial cables connecting the capacitors to the coil. The series inductance of the intervening spark-gap switch between the capacitor and diodes prevented the capacitor from effectively bypassing this transient to ground; the result was a very short but fatal overvoltage of the diodes. To prevent this transient damage, the diode strings were mounted directly across the capacitors, inside the capacitor cases. Maxwell Laboratories opened 12 of our 25 1.67 μF units and removed 20% of the parallel capacitance to make room for the diode strings. As a result, the individual units were reduced to 1.3 μfd, and the total bank to 16 μF.

The connection of the diodes directly across the capacitor introduces an additional complication. When a series string of diodes is subject to a transient reverse voltage, as was the case in the original connection, a simple ladder of small capacitors suffices to distribute the total voltage evenly among the diodes. However, with the direct capacitor connection, the D.C. charge voltage is applied to the string. In this case, grading of the voltage can only be done by a resistive ladder; the individual voltages will only become equal if the resistive ladder carries a current large in comparison to the variation of reverse leakage currents among the diodes themselves. For a random selection of ten production R620's, the required resistor current becomes unacceptably large. This problem was only soluble by careful selection of the members of each stack to match leakage currents at their peak reverse voltage. For the inventory of diodes available at the time this modification was made, it was only possible to assemble 12 stacks that could be assured of surviving together up to 19 kV. These were used in the Mark III thruster.

Another safegard necessary for the diode stacks is the insertion of a small series resistor. In the event of an accidental firing of the bank into the unloaded thruster coil, which has only a few milliohms of series resistance, a majority of the total voltage drop around the clamped secondary circuit would be the forward drop of the diodes themselves; as a consequence, most of the system energy (several kilojoules) would be deposited in the diodes, probably resulting in their destruction. Accordingly, a Nichrome wire resistor of 0.14 ohms has been inserted in series with each stack. This value is not sufficient to produce significant coupling between the capacitor and load circuits after clamping.

Figure 7.5 is a record of the load current when one capacitor-diode-switch module was fired into a high-Q inductive load at 25 kV. The high frequency and small amplitude of the ringing on the current trace just after the peak demonstrate that the clamping is very efficient. We conclude that the voltage reversal of the capacitor is probably no greater than 5%.

7.8 Capacitor Pressurization

When an otherwise well-manufactured and conservatively rated capacitor is placed into a vacuum environment, it can easily be destroyed unless special safegards are taken. To the extent that the unit has been well-impregnated and completely filled with oil, and to the extent that the case is even slightly flexible and the oil incompressible, the reduction of the external pressure to zero. will reduce the internal pressure of the capacitor to zero as well. The result will be boiling of the oil, the creation of vapor voids at points of electrical stress, and breakdown. In order to prevent such failure, each of the thruster capacitors has been additionally pressurized to 10 psi above ambient atmosphere; this will result in an internal pressure of 10 psi absolute in the vacuum environment.

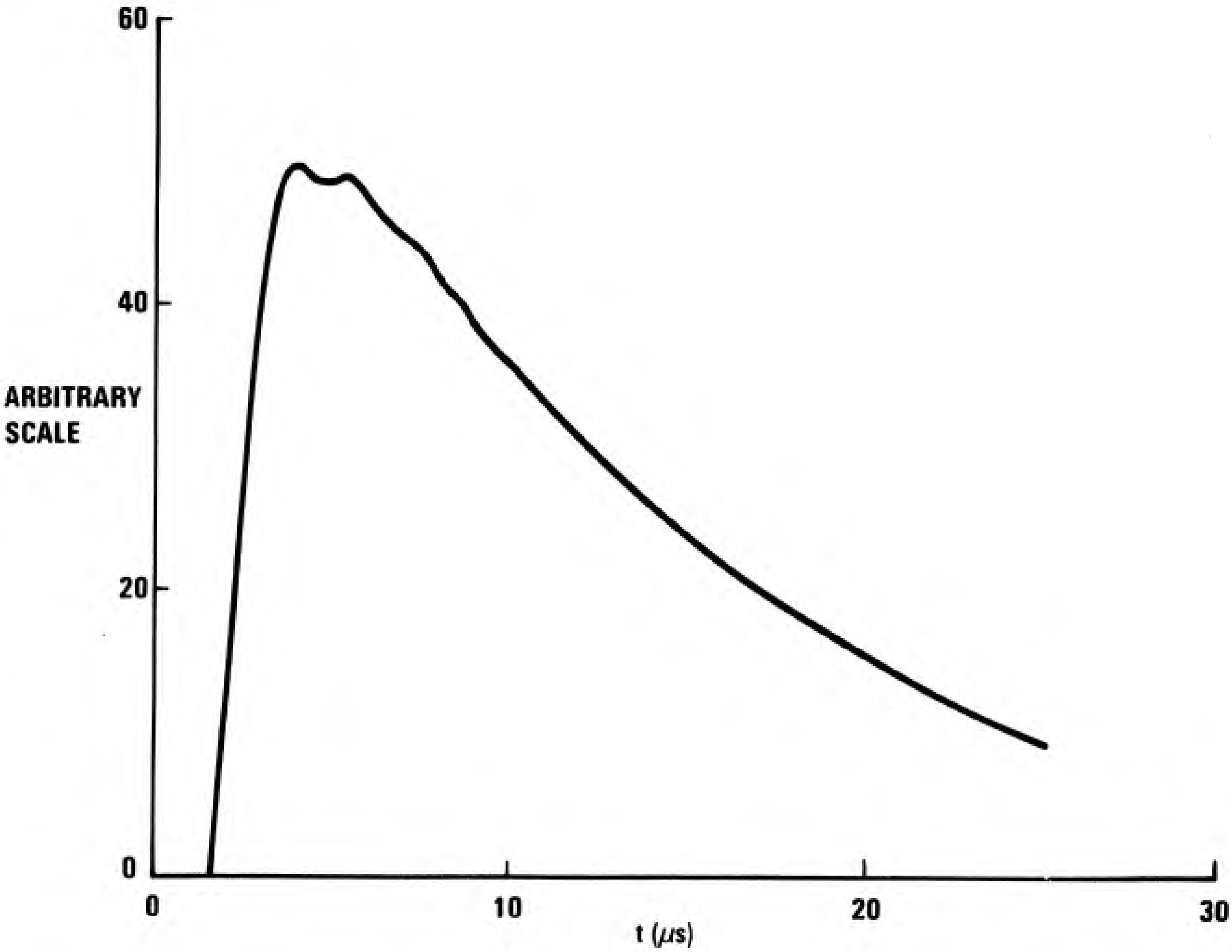

Figure 7.5 Diode-Clamped Capacitor Discharge Current (25 kV, 1.67 x 10^{-6}F, 10 Diode String)

8. DIAGNOSTIC MEASUREMENTS

While the fundamental measures of thruster performance are mass increment, stored energy, and mechanical impulse for each shot, this program has emphasized internal diagnostic measurements of the plasma as a means of understanding the way in which performance may be a function of such adjustable parameters as geometrical scaling, propellant species, or strength and time dependence of the driving magnetic field. Theoretical models of the overall thruster performance (Section 4) and detailed plasma behavior (Appendix A) have been developed; a comparison of diagnostic data with these should enable an understanding of the observed values of efficiency, I_{sp}, and impulse, as well as indicating paths to improved performance.

Ideally, a complete set of diagnostic measurements should include the electromagnetic group consisting of electric and magnetic field distributions in time and space as well as the current density distribution, and also the plasma group of ion and electron density, temperature, and velocity distributions, In addition, it is important to know the spatial distribution of injected propellant as a function of time.

8.1 Field, Current Density, Impulse; Mark I

Initially, on Mark I, distributions of magnetic field, current density, and propellant were measured. The field and current suffice to give a figure for total impulse when their vector cross-product is integrated spatially and temporally; and they also allow a determination of the uniformity with which force and impulse are delivered to the plasma over the surface of the coil. The time evolution of the advancing magnetic field, when compared to the one-dimensional MHD model of Appendix A gives an indication of plasma resistivity, and thus a measure of the degree to which field diffusion competes with convection in limiting efficiency.

Current density in the plasma and coil is purely in the azimuthal direction (j_θ); consequently the magnetic field has only radial and axial components. Since only the axial (z) components of force density have a non-zero spatial integral, it is sufficient to measure B_r and j_θ to derive F_z and impulse.

8.1.1 Probes

In principle, one may determine current density by measurement and differentiation of the distributions of all field components. However, the attainment of suitably accurate derivatives requires the sampling of B_r on a much finer spatial grid than would otherwise be necessary. The method chosen for these experiments was to measure j_θ directly by use of a "Rogowski coil" probe, a miniature toroidal coil whose output voltage is proportional to the time derivative of the total current flowing through its opening. Magnetic field was sampled with a conventional miniature multi-turn loop probe.

8.1.2 Sampling and Recording

The outputs of both these probes were integrated by a passive RC network and recorded on an 8-bit digital transient recorder. A typical record consisted of 250 samples, taken at either 50 or 100 nanosecond intervals. Immediately after each shot of the thruster, the digital record was transferred to disk storage in the system computer.

Spatial sampling of the fields was done on a 90-point grid in the R-Z plane. Six radii, covering the range from 25 to 50 cm in 5 cm intervals, were used. The Z coordinates were non-uniformly spaced; the six points nearest the coil were at 5 mm intervals from .5 cm to 3 cm, the next five at 1 cm intervals from 4 to 8 cm, and the last four at 2 cm intervals from 10 to 16 cm. In this way, resolution appropriate to the structure of the field was available throughout the acceleration stroke.

A complete data run consisted of: 1) 90 B_r records, 2) 90 j_θ records, and 3) 90 dummy records for which the aperture in the Rogowsky probe was closed but the probe scanned over the grid in the nominal way. The latter was necessary because of the particular susceptibility of the probe to spurious signals. It is, in effect, a differential probe whose output is the difference between two neighboring loops while noise from capacitive effects, or magnetic pickup from leads, tends to be additive. Since no current can pass through the Rogowsky in the dummy condition, its output is pure noise characteristic of the probe condition. In the processing of data, these dummy records were subtracted from the normal open-coil records.

8.1.3 Data Processing and Analysis

For the processing and analysis of these data, a number of computer programs were written. The 90 raw records were typically taken at a variety of gains and baseline offsets, depending upon the magnitude and shape of the signal at particular grid points. Data on gain, offset, timestep and run number were appended to each disk record by the logging programs (BLOG, JLOG,GASLOG) which also provided a graphic display of the transient recorder contents and allowed either for rejection of the new record in the event of equipment malfunction or acceptance for storage. Values of probe calibration constants and integrator time constant, common to all the points in a run, were input to the processing routines.

A typical processing sequence (program IMPULS) is:

1) Subtract J noise records from total J.

2) Normalize gains and subtract baseline offsets, J and B.

3) Take JB products over all cells to create a force density matrix.

4) Integrate force density over space to get total force as a function of time.

5) Integrate force over time to get total impulse.

Another diagnostically useful routine (FCONT) produced contour maps of force density as a function of time using the matrix produced in step 3), above. Reversal of steps 4) and 5) allowed a mapping of the total impulse per unit area, as a function of position over the coil.

8.1.4 Experimental Data, Mark I

Data on field, current, and force density distributions taken on Mark I at 22 kV bank voltage with argon propellant are shown in figures 8.1-8.3.

Figure 8.1a shows two records of the radial magnetic field as a function of time, taken at Z=1 cm and Z=5 cm, both records at a radius of 40 cm. The Z=1 cm record is very closely similar to the total circuit current, and displays a shape characteristic of efficient transfer of bank energy to the

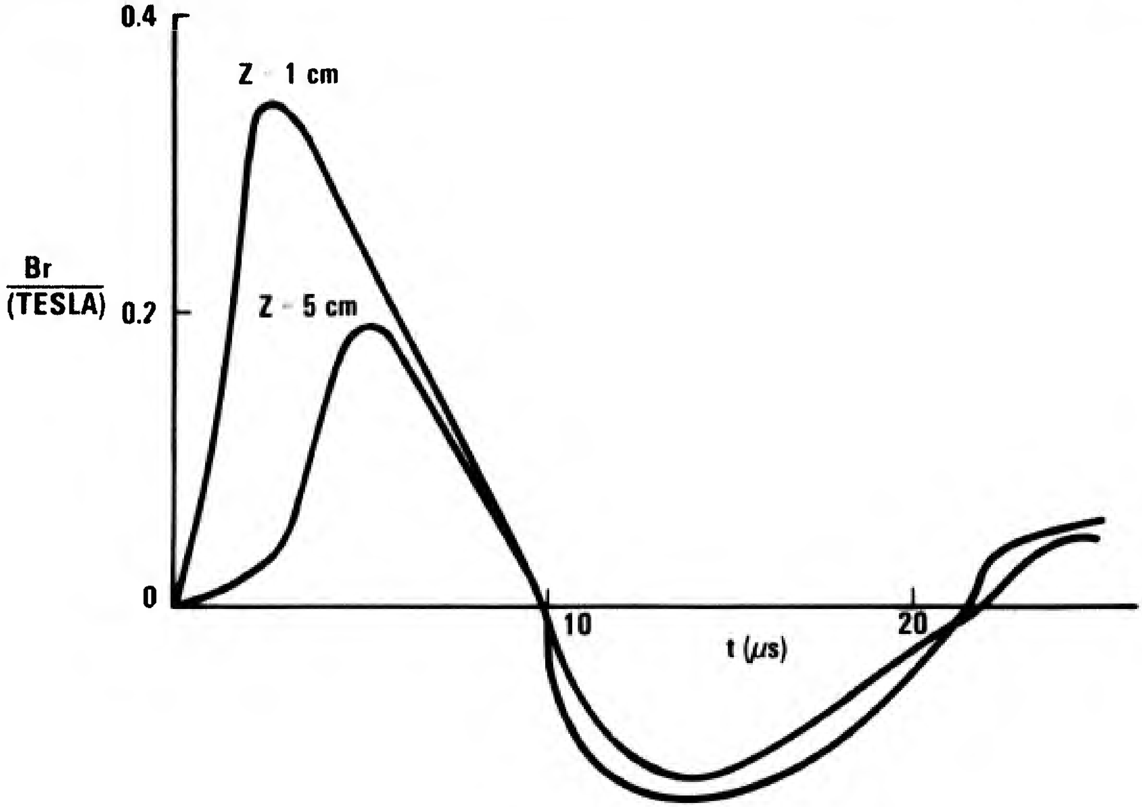

Figure 8.1(b) Current Density Variation With Time (Mark I, 22 kV)

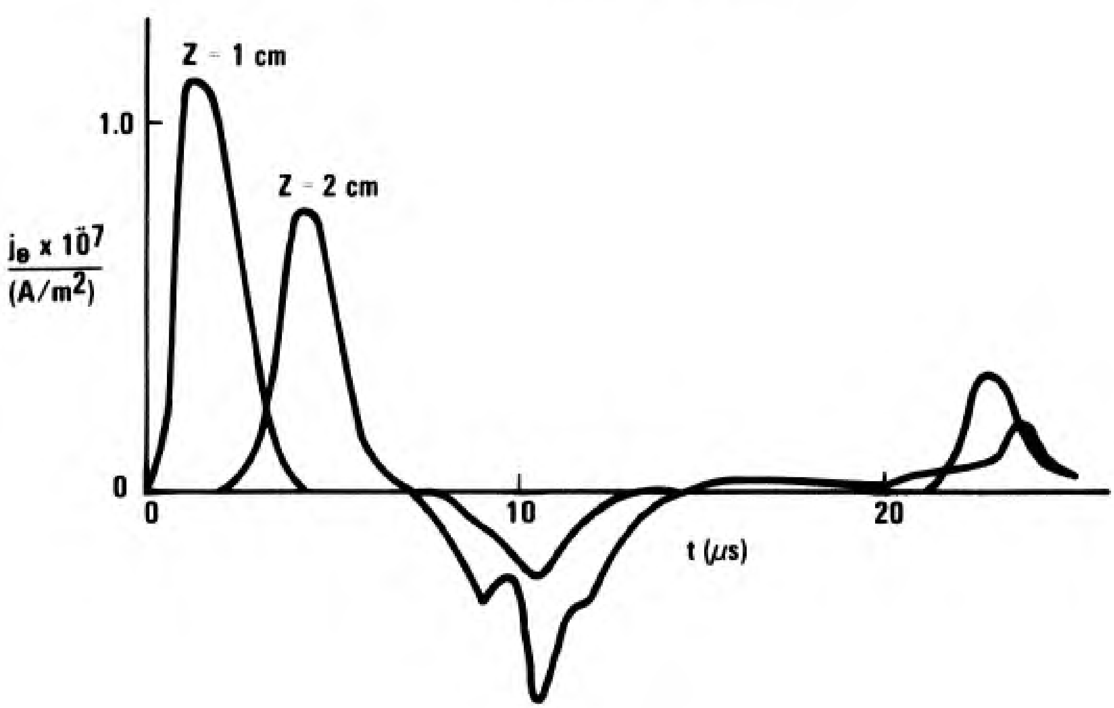

Figure 8.1(a) Magnetic Field Variation With Time (Mark I, 22 kV)

load, i.e., it is extremely asymmetrical around its first maximum. The risetime is just over 2 microseconds, a result of the low inductance from the well-coupled load, while the drop to the first zero takes an additional 8 microseconds indicating the large inductance rise associated with the acceleration stroke. The acceleration of a second plasma sheet away from the insulator produces a similar if less extreme asymmetry in the second half-cycle of the current.

At Z=5 cm, the field rise is delayed by the shielding effect of the intervening current sheet nearer the coil. As the current sheet passes the probe position the field rises to nearly the same value it has at Z=1 cm, indicating that the remaining plasma discrepancy between the two locations is small. The slight discrepancy between the two curves during the second half-cycle indicates the acceleration of a small but not negligible additional mass from the region close to the coil.

Current density at these same locations is shown in Fig. 8.1b. Three distinct current pulses are seen at Z=1 cm. Each pulse after the first results from a new breakdown of residual gas at the insulator when the electric field reverses. Little mass is accelerated by these secondary currents; they serve mainly to separate regions of oppositely directed magnetic flux.

A cross-plotting of the field and current time series gives distributions of field and current as a function of position at assigned times. Examples are given in Fig. 8.2.

Fig. 8.2a displays $B_r(z)$ for times of 2,4, and 6 microseconds. On the assumption that B_r does not vary strongly as a function of R in this region, the slope of the curves may be taken as current density. The actual Rogowsky data of 8.2b are seen to bear this out. The thickening of the current sheet which results from plasma resistivity is evident in this series.

The long "toe" of B_r (z) extending ahead of the advancing current results from field leakage through the sheet. The weak toe at t=2 microseconds is probably vacuum field that was deposited prior to full development of the first breakdown, while the substantial downstream field at t=6 is a result of resistive B_r diffusion. Note that the slope of B_r is not accompanied by current density in the 10 to 16 cm region; here, curl B is made zero by an additional radial derivative of B_z.

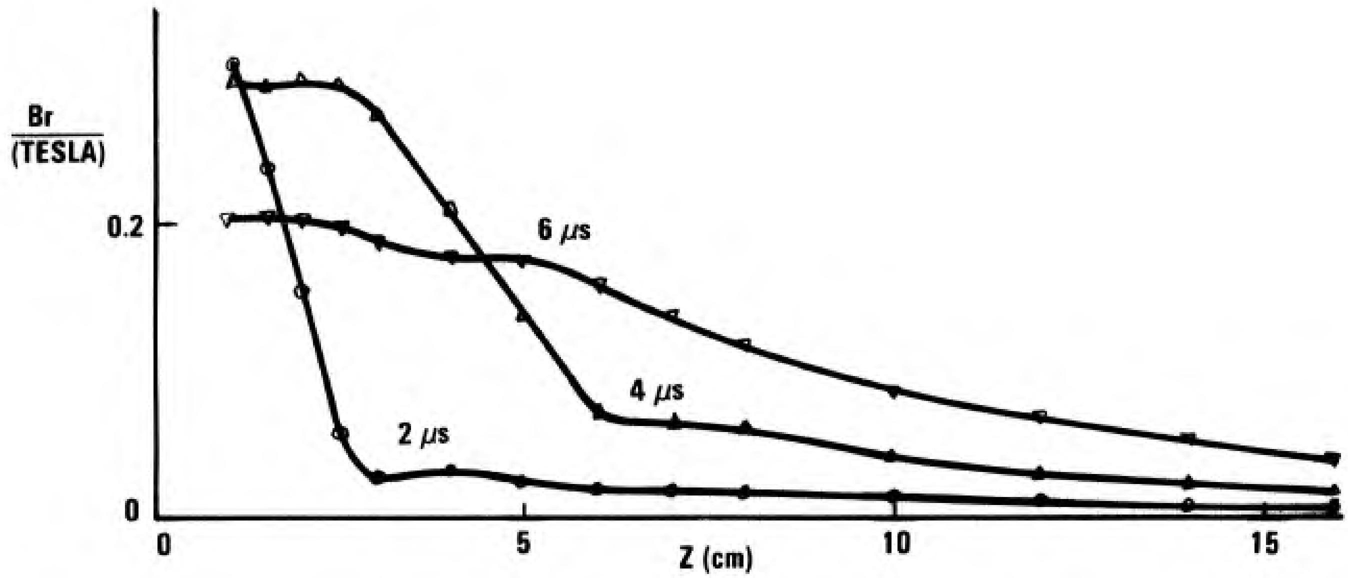

Figure 8.2(a) Axial Magnetic Field Distribution (Mark I, 22 kV)

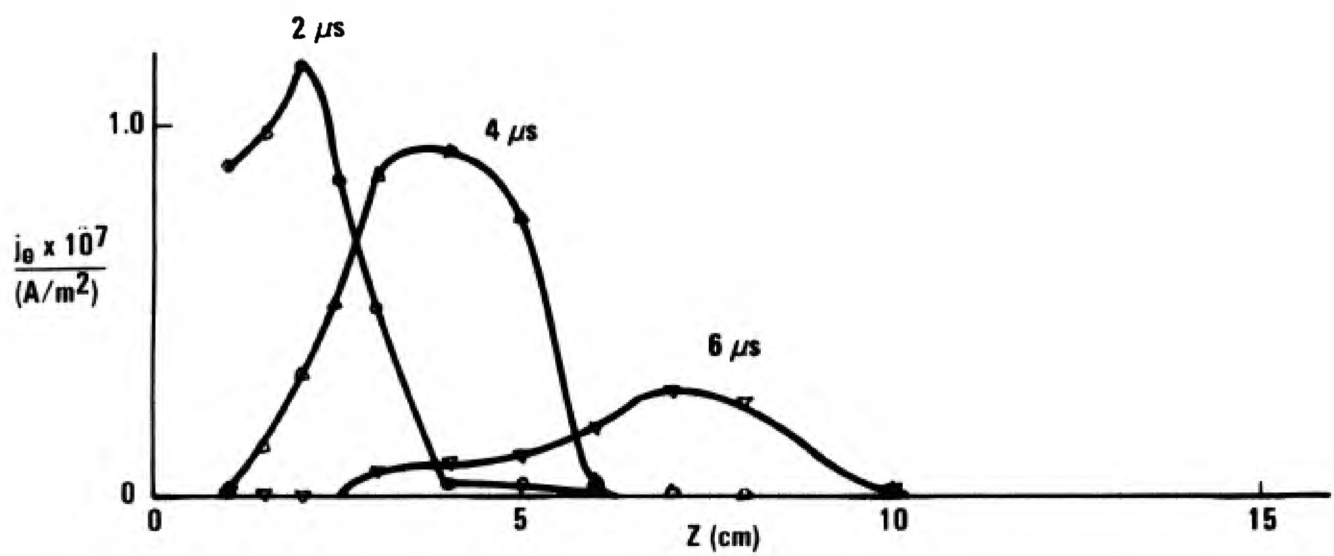

Figure 8.2(b) Axial Current Density Distribution (Mark I, 22 kV)

The degree of field diffusion seen here corresponds approximately to the theoretical case (Appendix A) for a resistivity of 5×10^{-4} ohmmeters, this resistivity by itself should not be responsible for lowering efficiency below 50%.

Contour maps of force density in the R-z plane are given in Fig. 8.3 for times of 2 and 4 microseconds. In this instance, the largest density lies in the radial zone between 30 and 40 cm. However, this maximum is not very peaked, and the contours are generally flat out to 50 cm. Below 25 cm, little force is generated; the reason is that the initial gas density in this zone was small.

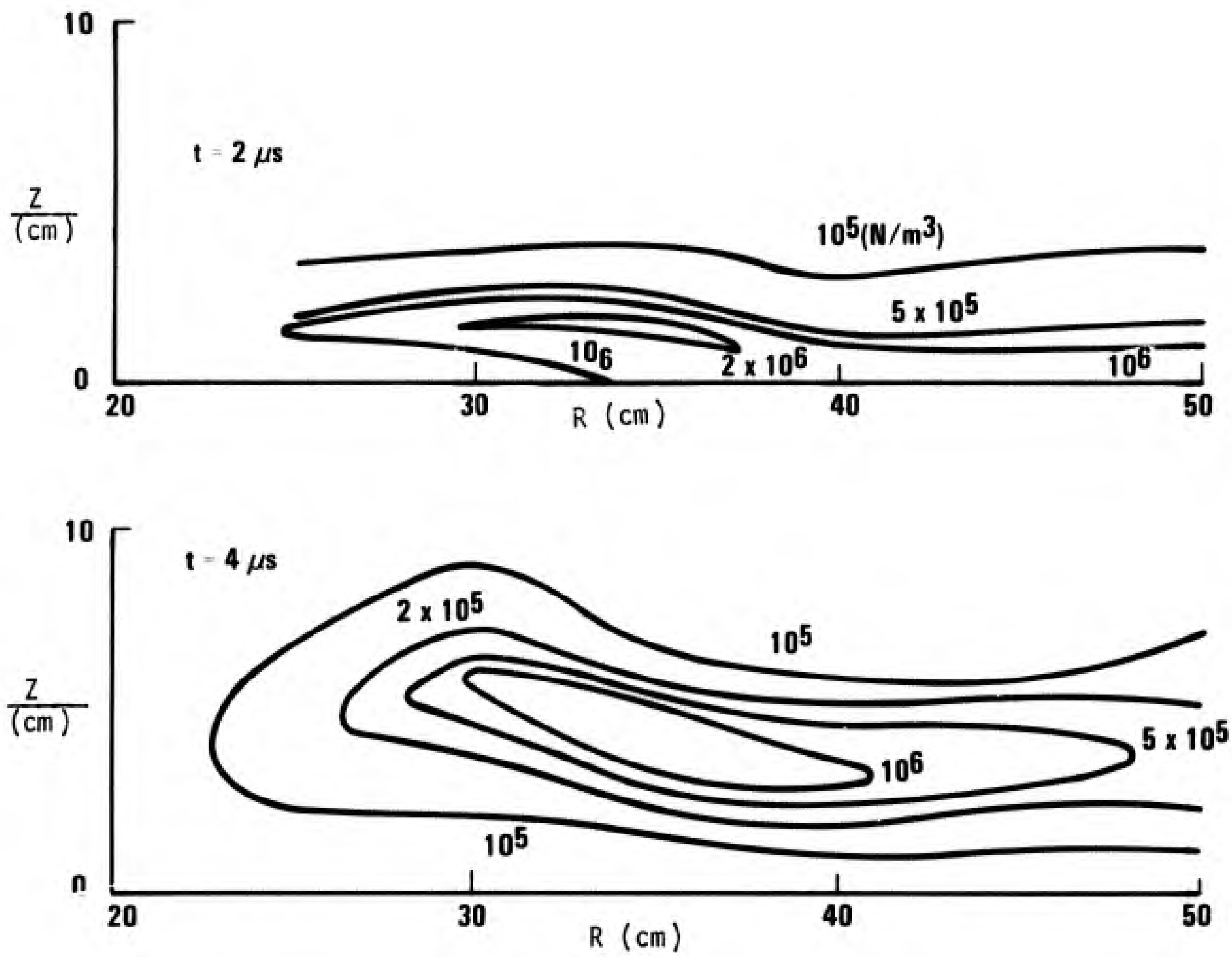

Figure 8.3 Force Density Distribution at Two Times (Mark I, 22 kV)

9. THRUST BALANCE PERFORMANCE DATA

9.1 Mark I

The ultimate performance of a pulsed thruster is determined by combining the three fundamental parameters of energy increment, mass increment, and impulse. It is desirable that each of these be itself measured by the most fundamental and straightforward means available. In the case of impulse, a direct mechanical measurement is clearly necessary.

9.1.1 Thrust Balance

The thrust balance used for the Mark I measurements consisted of a horizontally aligned beam having the thruster attached to one end and a counterweight to the other, mounted on a vertical torsion bar through its center. The torsion bar was fastened to the inside wall of the vacuum tank. The torsional oscillation period of the assembly when loaded with the 300 kg combined masses of thruster and counterweight was approximately 9 seconds; typical deflection from a thruster shot was 1 mm at the beam end, or approximately 1 milliradian of angle. The deflection transducer was a differential transformer whose movable armature was attached to the beam 20 cm from the rotation axis. Utility lines servicing the thruster were brought in along the rotation axis in such a way as to cause little damping of the balance. Q of the oscillation was usually over 100, which necessitated the use of a separately applied damper to bring the beam to rest once a reading of impulse had been taken.

Calibration of the impulse response of the balance was accomplished by the use of a bar pendulum. The .25"x1" aluminum bar was pivoted directly above its impact point on the thruster axis at the center of the gas valve, at a vertical distance equal to 2/3 of its 82 cm length. For this position on a bar pendulum, impact produces no corresponding reaction at the pivot, and consequently the entire momentum of the rod is delivered to the thruster. It is also necessary to insure that the impact is inelastic; otherwise the rebound velocity of the pendulum would have to be accurately determined. A simple putty cushion was adequate for this function. Under these conditions, the delivered impulse is given by

$$\Delta I = \frac{m}{2} \left(3 \text{ g} l \left(1 - \cos \Theta_0\right)\right)^{\frac{1}{2}}$$

where Θ_0 is the starting angle from the vertical, and it is assumed that impact occurs at $\Theta=0$.

9.1.2 Experimental Results

Mark I impulse data were taken for both Ar and NH_3 propellants and for bank voltages between 20 and 26 kV. Runs were also made with half of the capacitors removed in order to ascertain whether a closer matching between bank period and stroke time would have a substantial effect on efficiency.

The results for argon and the full bank are as follow:

Table 9.1 (a) Argon Thrust Balance Data

Mass (kg)	Voltage (kV)	Impulse (N-S)	I_{sp} (Sec)	Efficiency
1.2×10^{-5}	24	0.196	1734	0.285
1.2×10^{-5}	26	0.214	1897	0.291
1.5×10^{-5}	24	0.221	1562	0.289
1.5×10^{-5}	26	0.236	1670	0.282
1.8×10^{-5}	18	0.165	964	0.237
1.8×10^{-5}	24	0.228	1334	0.255
1.8×10^{-5}	26	0.260	1521	0.282
2.0×10^{-5}	24	0.240	1228	0.247
2.3×10^{-5}	24	0.263	1171	0.259
2.6×10^{-5}	16	0.140	551	0.146
2.6×10^{-5}	18	0.185	721	0.201
2.6×10^{-5}	20	0.208	816	0.205
2.6×10^{-5}	22	0.246	966	0.237
2.6×10^{-5}	24	0.264	1036	0.229
2.6×10^{-5}	26	0.292	1147	0.239

Table 9.1(b) Ammonia Thrust Balance Data

Mass (kg)	Voltage (kV)	Impulse (N_s)	I_{sp} (Sec)	Efficiency
5.0×10^{-6}kg	20	0.109	2220	0.296
5.0×10^{-6}kg	22	0.123	2476	0.304
5.0×10^{-6}kg	24	0.138	2766	0.319
6.5×10^{-6}kg	20	0.107	1670	0.210
6.5×10^{-6}kg	22	0.124	1940	0.240
1.2×10^{-5}	22	0.157	1360	0.213
1.2×10^{-5}	24	0.163	1413	0.193

These combined data, together with points taken with the half-capacitance bank, are plotted in the efficiency vs. I_{sp} curve of Fig. 9.1.

It may be noted that the efficiency with argon propellant tends to saturate at about 30%, and does not increase significantly with I_{sp} above about 1500 seconds. Ammonia, giving smaller efficiency than argon under 2000 seconds, continues a rising trend with I_{sp} and finally shows the highest efficiency of any of the data.

Decreasing the bank capacitance has had negligible effect on the efficiency trend of argon except to allow operation at lower I_{sp}. With ammonia however, the curve is clearly moved upward.

The practical problem with moving upward along this curve toward higher I_{sp} with the present thruster is that it would require either higher voltage than could be supported by the capacitors, or else a mass loading so light as to make uniform breakdown unlikely.

9.2 Repetitive Firing Demonstration

The capability of the power supply, control system and thruster to operate repetitively was demonstrated with the Mark I thruster. The test burst consisted of 10 sequential firings in a period of 1 second.

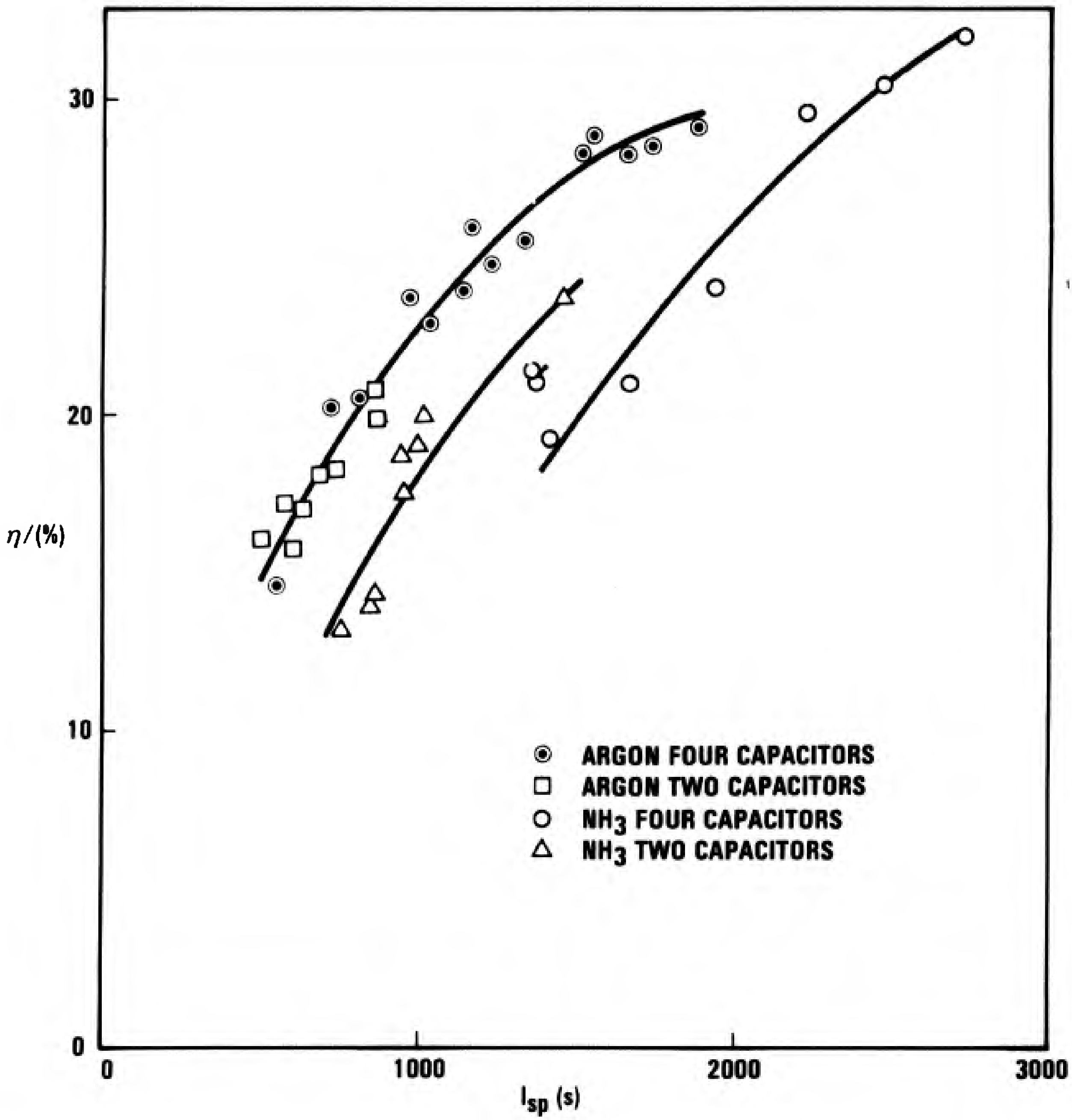

Figure 9.1 Thruster Balance Data for Argon and NH_3 (Mark I with 2 and 4 Capacitors)

10. MARK II THRUSTER

10.1 Design

While the Mark I thruster has produced performance figures on single shots, there are several features of its design that would preclude sustained and reliable repetitive service.

1) The four 5 μF capacitors are tied together and to the load through a single spark gap switch. A generally accepted figure for tungsten spark gap erosion is 10 micrograms per coulomb of charge transfer. For this bank, charged to 20 kV and operated 10^8 times (the nominal number of shots for LEO-GEO cargo transfer), the resulting electrode mass loss would be 400 grams, or an order of magnitude more than the total present mass of the electrodes.

2) The failure of one of the capacitors would amount to a failure of the entire bank, since they are tightly paralleled.

3) The single spark gap is a point of concentrated power loss and requires vigorous cooling. At a nominal drop of 100 volts, it dissipates 400 watts for a thruster & repetition rate of 20 hertz.

All of these problems are solved by a redesign of the system in which the capacitor bank is subdivided into significantly more than four capacitors, with each capacitor individually switched and capable of disconnection from the rest of the bank in the event of its failure. The Mark II design employed twelve capacitors of 1.67 microfarads each. They were specially constructed with terminal bushings on each end of the case, which allowed convenient placement of the switches at the outside of the bank, while the coaxial cables from the capacitors to the coil terminals could still be kept short enough to minimize parasitic inductance. A schematic representation of one of the twelve modules is given in Fig. 10.1. Each of the spark gap electrodes was sufficiently massive to allow of the order of 10^8 shots. Thermal cooling of each gap was provided for by the direct connection of one of the electrodes to ground, and the thermal conduction to ground from the second electrode through the capacitor.

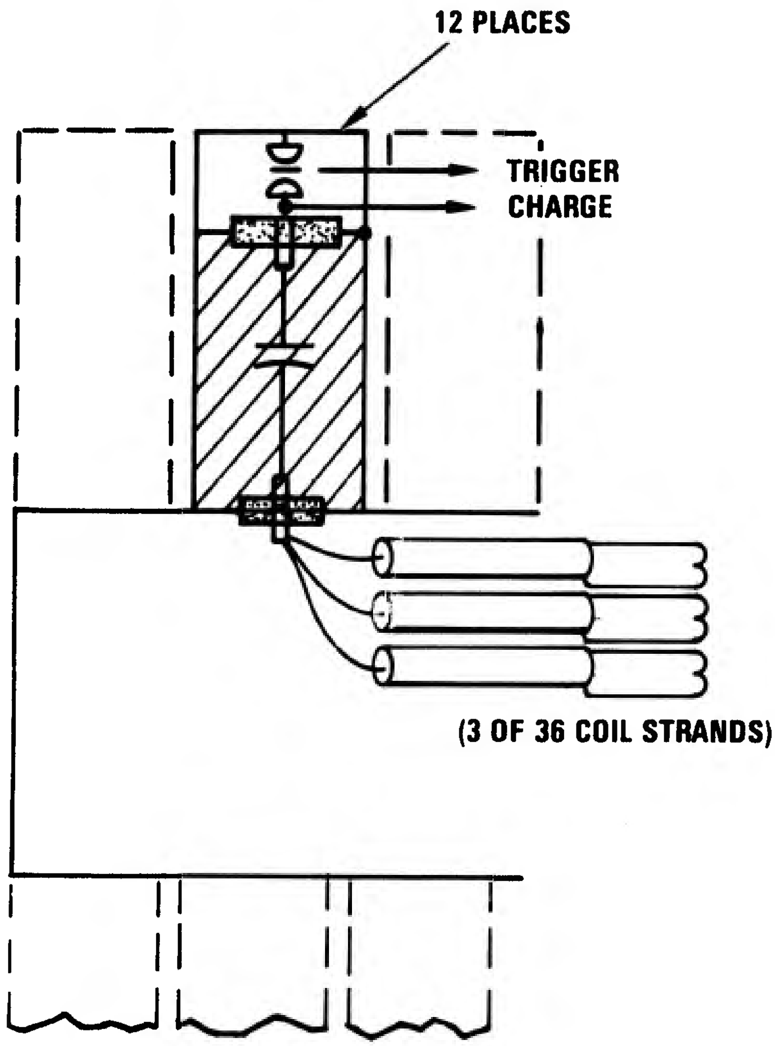

Figure 10.1 Mark II Bank Module

Charging of the bank was accomplished through the network shown schematically in Figure 10.2 .

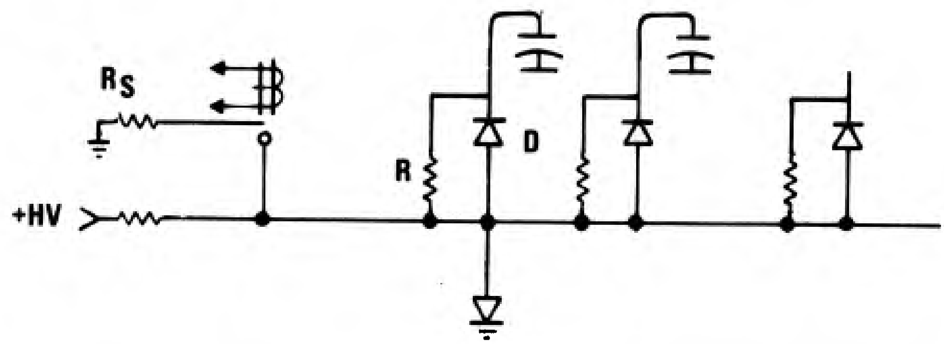

Figure 10.2 Charging Network

Each capacitor was isolated from the rest of the bank by diode D and parallel resistance R of 10^5 ohms. In the event of failure of a capacitor, the flow of energy from the rest of the capacitors into the fault was blocked by their individual diodes; resistances R allowed for slow discharge ($\sim$ 0.1s.), and release of the energy into the resistors themselves. The main power supply dumping resistor R_S was also 10^5 ohms; on ordinary discharges through the shorting relay the main bank energy was therefore consumed in R_S rather than in the smaller protective resistors.

Triggering for the 12 gaps was provided from a master trigger gap connected accordingly to Fig 10.3

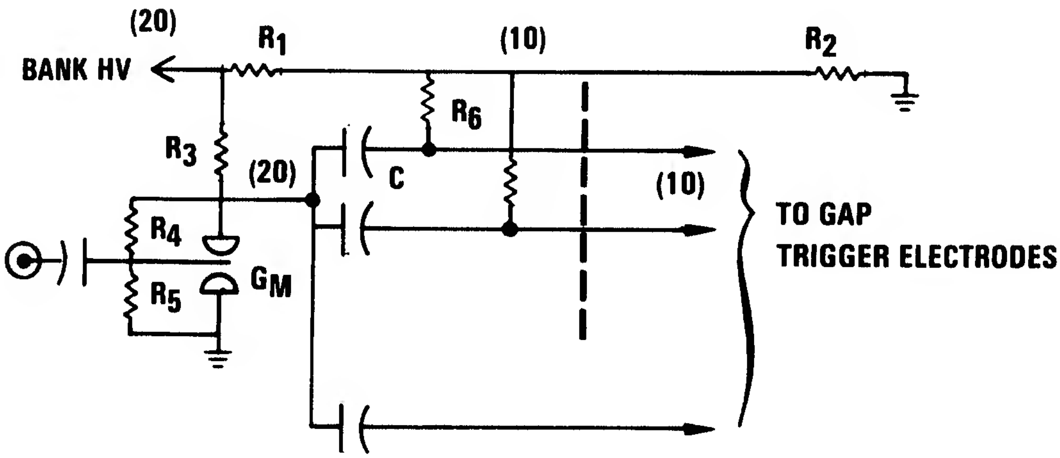

Figure 10.3 Master Trigger Gap Schematic

Resistors R_1 and R_2 divide the bank high voltage (shown here as 20 kV) by half to 10 kV for bias of the gap triggers. Resistors R_6 isolate the gap triggers from one another to prevent destructive circulating currents in the event of misfire or failure of one capacitor. R_4 and R_5 bias the trigger of master gap G_M. When G_M is fired,, the left-hand bus connecting capacitors C drops from +20 kV to ground, and so the trigger lines drop from +10 kV to -10 kV, tripling the stress on one side of the main gaps and causing breakdown.

A photograph of the Mark II capacitor bank is shown in Figure 10.4. This 3/4 rear view shows 6 of the 12 pulser modules with the spark gaps mounted on top of the capacitors supplied by gas inlet and exhaust lines and by individual charging and trigger cables.

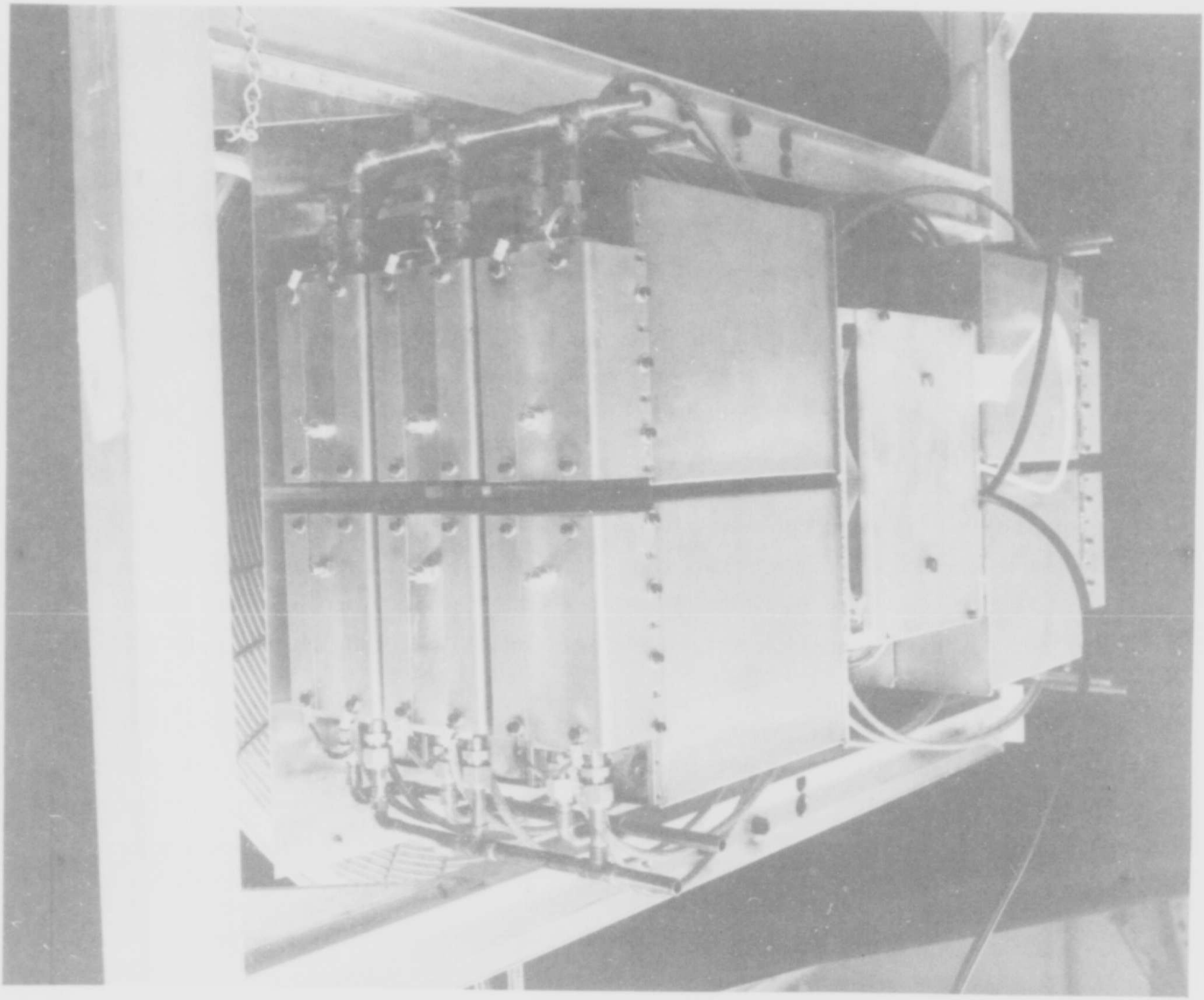

Figure 10.4 Mark II Capacitor Bank

10.2 Thrust Stand

The additional weight of the Mark II bank made it impractical to continue use of the swinging-beam thrust balance employed for Mark I. Accordingly, a new and more compact thrust stand was designed and constructed.

The stand consists of a pair of rectangular aluminum I - beam frames connected at their four corners by vertical stainless steel straps that act as spring flexures. When such a flexure is loaded from the top by a weight its effective first-order spring constant is decreased due to the fact that the loading mass is lowered as the spring is bent to the side, and thus its potential energy is lowered. As loading mass is added, the restoring spring constant decreases finally reaching zero at "critical" loading. Provided that sufficient care is taken in leveling such a stand one can achieve almost any desired level of sensitivity.

The stand has the additional merit of being extremely compact, occupying a horizontal area approximately two feet square, with an overall height of seven inches. It was mounted on the bottom of the Mark II thruster as a permanent component of its structure. It is a decided advantage, in the event that the thruster were to be tested at a remote facility, to have the thrust and impulse instrumentation actually a part of the thruster assembly.

Displacement of the thrust stand was measured by an optical lever in which a focusing mirror, mounted on the thruster, relayed a He-Ne laser beam, incident from outside the vacuum tank, back to a solid-state quadrant detector, also outside the vacuum. Adjustment of the thrust stand leveling was done mechanically through rotating vacuum seals.

Calibration was by means of a directly applied steady force, transmitted from a weight hanging by a thread over a pulley

10.3 Mark II Experiments

Initial measurements of bank performances were made with a stainless steel sheet dummy load placed over the coil. Synchronization of the spark gaps appeared to be adequate. Tests of the bank with and without diode clamps were made. This series of experiments demonstrated that while a diode clamp placed downstream of the circuit switch could perform well on a single module in a test fixture, cable reflections from the actual coil load applied fatal overvoltage to the diode strings in the thruster (of Section 7.7). At this point, a decision was made to incorporate the diodes within the capacitors themselves (Mark III configuration). In the interim Mark III was placed into the vacuum tank for testing without diode clamps.

The new thrust stand allowed the thrusters to be installed coaxially with the vacuum tank, thus allowing a larger drift space for the accelerated plasma, and much easier access to all parts of the thruster. The gap between the tank wall and the outer diameter of the thruster coil was smaller than desirable, amounting to only about 11 cm in radius. A computation of the perturbation by the tank showed an 8% inductance decrease of the unloaded coil. This was judged to be significant in that it could result in an impulse decrease by a slightly smaller factor; however the data are correctible for this error.

During preliminary shots, impulse appeared to be erratic, with some large values, and subsequently, very small and fluctuating values. Inspection of the thruster revealed that the main coil had suffered a catastrophic failure; explosive short-circuits had occurred at the feed points of a majority of the strands. The probable sequence of events is that a single such failure propagated itself by mechanically shocking and fracturing the Lucite insulation at the feed points of neighboring strands. The initial fracture of the coil structure may have been caused by hammering of the dummy load plate used earlier when it had been clamped against the coil surface to simulate the plasma for thruster operation outside of the chamber.

The failure was judged to be irreparable. Several of the Litz wire strands had been totally ruptured and there seemed to be no prospect of restoring the integrity of the insulation layer between conductors at the feed-points.

An older thruster coil, wound with 3/16" copper tubing, was available, and was installed on the thruster in order that experiments might continue. This coil differed from the original one in having no edge compensation, but rather a uniform current density over its entire surface.

At the time of the re-installation of the coil, the capacitors containing diode clamps were delivered, and these were installed as well. We designate this version of the thruster Mark III.

10.4 Mark III Thruster

Initial operation of Mark II gave disappointing values of impulse as well as some irregularity. It was found at this point that a serious amount of "jitter", or lack of synchronism, had appeared among the various capacitor switches and that as a result substantial energy was being lost in current circulation between capacitors in the bank. It was decided at this point, and for the purpose of at least obtaining definitive data on clamped operation of the full bank, to convert the thruster back to a single spark-gap switch. The Mark I switch was serviceable and the conversion straight forward.

10.5 Mark III Experiments

With single point switching, successful clamped bank operation was achieved. When the diode strings used in the capacitors were being assembled and tested for reverse leakage as a function of voltage, one of the twelve strings showed a substantial reverse leakage at 19 kV. It failed after approximately 200 shots. A second unit failed because of a manufacturing error, in which insulation placed betwen the diode string and the capacitor case broke down. The remainder of the bank worked reliably through the remainder of the program.

Impulse delivered by Mark III continued quite low. Efficiency and I_{sp} remained below 10% and 1000 seconds, respectively. A magnetic probe run showed that, in contrast to Mark I at the same voltage, very poor quality current sheets were being formed. Breakdown was slow and as a result, substantial field energy leaked ahead of the current.

10.6 Electric Field Distributions

The poor current sheet formation obtained in Mark III is suggestive of inadequate initial E_{Θ}. A strong possibility for the cause of this condition is that: 1) the placement of the coil and the tank on the same axis drives down E_Θ at the outer radii of the coil where most of the propellant lies, and 2) the lack of compensating windings on the replacement coil further reduces E_Θ at large radii. It should be recalled that since Mark I was mounted transversely to the tank, the coupling of the tank to the coil was very small, so E_Θ should have suffered very little depression.

These possibilities were tested in an explicit numerical computation of the vector potential, electric field, and magnetic field in the region of the coil as mounted in a perfectly conducting surrounding tank.

The computation exploits the fact that in an axisymmetric system having purely azimuthal current, the vector potential is itself only azimuthal, and obeys Poisson's equation:

$$\nabla^2 A_\Theta = -\mu_0 J_\Theta$$

This can be solved numerically on a grid in the r-z plane by use of a Gauss-Seidel relaxation scheme. For the thruster case, a 1000-point grid was used. Current density corresponding to both the compensated and uncompensated coils was applied to the appropriate cells, and solutions were obtained for both the actual tank radius, and for a hypothetical tank of 7 inches larger radius where the coupling effects should be greatly reduced. E_Θ is simply the time derivative of the vector potential; therefore the distribution of vector potential is similar to the distribution of E_Θ.

Figure 10.5 shows the distribution of A_Θ for the two cases of interest here: (a) the compensated Mark I coil with a 31 inch radius "pseudo-wall", i.e., in an essentially unperturbed state as when transversely mounted in the tank, and (b) the uncompensated copper tubing coil as actually mounted in the 48 inch tank. The same coil current is assumed in both, a reasonable assumption since the inductances are not greatly different.

It is clear that A_Θ has dropped considerably over the outer half of the tubing coil, while it is well sustained at a high level over the whole of the original coil. Since the electric fields used in Mark I were only marginally larger than necessary to produce good quality current sheets, we conclude that the poor performance of Mark III is attributable to the inadequate substitute coil and the undersized vacuum chamber in combination driving E_Θ to values below those necessary for good breakdown. It is most important to emphasize that this behavior is not attributable to any intrinsic short coming of the thruster itself.

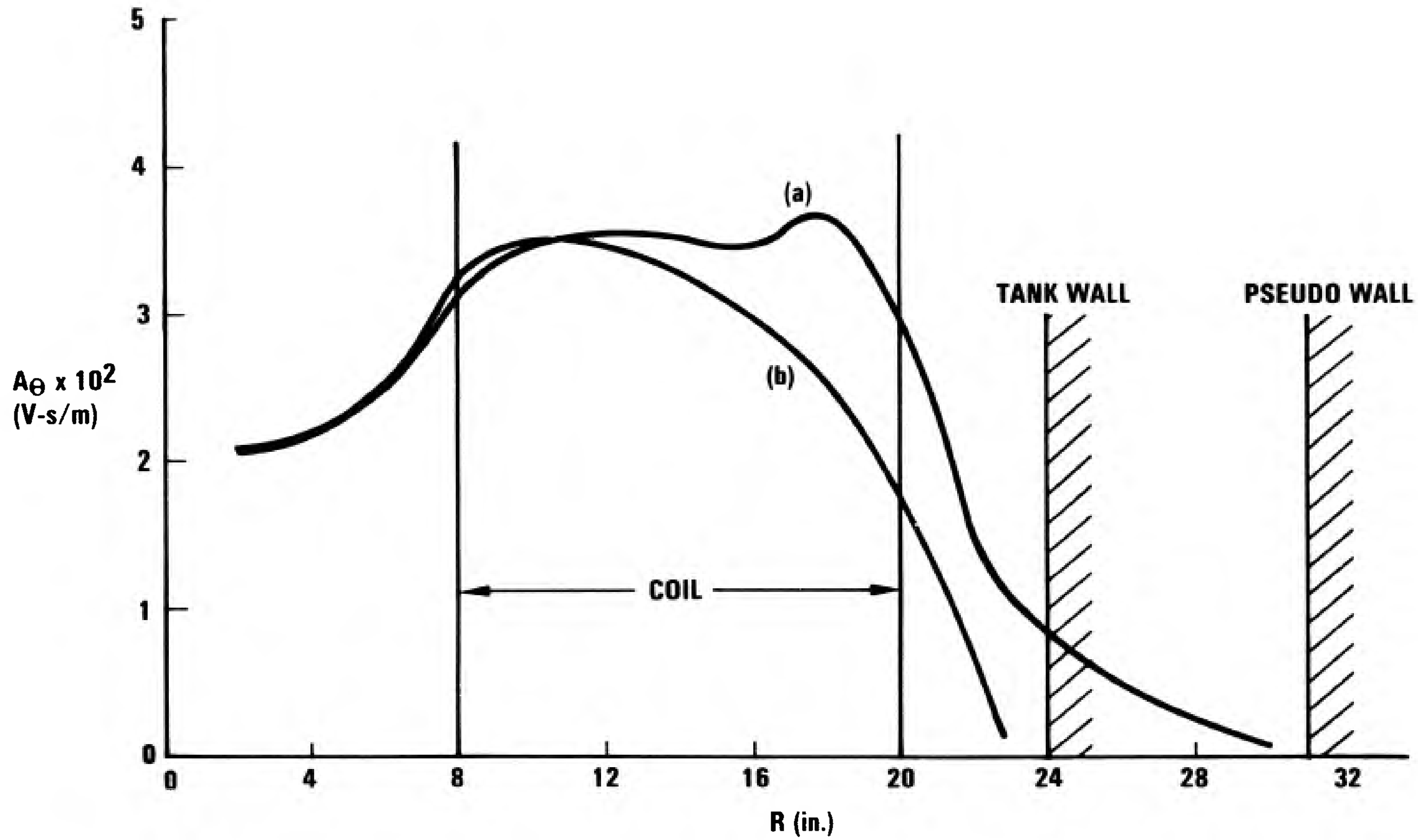

Figure 10.5 Comparison of Vector Potential for 2 Thruster Coils

11. MARK IV THRUSTER

The Mark IV thruster design is a continuation of the concepts explored in the prior configurations. It is scaled to a larger diameter to accomodate the high power requirements of multimegawatt Electric Transfer Vehicles (ETV), and also to benefit from the increased efficiency of a larger diameter.

11.1 Thruster Design Parameters

11.1.1 Propellant

Hydrazine is an attractive propellant for a practical thruster. Its atomic weight is comparable to argon (32 compared to 40 for argon) so that the gas dynamics of injection should be essentially the same.

From gas density measurements with the 1 meter coil, the injected gas is fairly well confined in a 2 cm layer over the coil. If this fill depth scales as the coil diameter, the mass per pulse would vary with the cube of coil diameter.

As an example of a large coil, the O.D. is assumed to be 2 meters with an I.D. of 0.67 meter and a fill depth of 4 cm, a propellant volume of 0.112 m^3. Experience with previous thrusters has shown that fill densities less than 1.5×10^{22} per m^3 do not form compact plasma current sheets. For this minimum number density of hydrazine gas, the mass per discharge for the assumed 2 meter thruster would be 9×10^{-5} kg. Its kinetic energy at 2500 seconds I_{sp} would be 27 kJ and the capacitor bank energy for 50% efficiency would be 54 kJ. At a pulse rate of 10 Hz, the power would be 0.54 mW, at 50 Hz it would be 2.7 mW. Corresponding values at 3000 seconds I_{sp} would be 1.22 and 6.1 mW. Thus a 2 meter coil diameter would be an appropriate scale size for a thruster operating with hydrazine gas at powers in the range of 1 to 5 mW, at 10 to 50 Hz and at I_{sp}s of 2500 to 3000 seconds.

11.1.2 Pulser Circuit

The induced EMF that ionizes the injected gas and drives the plasma current sheet, must be the same for all thruster sizes. Consequently, for the 2 meter Mark IV coil, this becomes 50 kV to produce the same azimuthal electric field as that of the 1 meter thruster at 25 kV. An inductive Marx bank approach is used to reduce this to a more convenient value for capacitor operation. This is done by dividing the coil into 4, 90° sectors, for example, each having a capacitor storage voltage of 12.5 kV. The capacitors in each sector are charged in parallel to 12.5 kV, and fired at the same instant to produce 50 kV around the plasma current loop.

The capacitors used in the Mark IV pulser would be the all-film polypropylene designs described earlier. As an example, six capacitors might be used in each of the sectors, making a total of 24 for the thruster. Each capacitor would be switched by a string of solid state thyristers (Westinghouse RBDT) and clamped by a diode string as in the Mark III.

11.1.3 Thruster Configuration

Figure 11.1 shows a preliminary component arrangement for a 3 meter example of the Mark IV type thruster. The propellant injector is placed farther from the coil than it was in the 1-meter thruster. This increases the axial momentum of the injected puff of gas while reducing its radial momentum, and it also reduces the difference in arrival time of the gas at the inner and outer coil radii so that less time is available for radial drift. These differences should produce a more compact and uniform gas distribution over the coil when the thruster is fired, resulting in some performance improvement. Figure 11.1(b) shows the arrangement of the pulser components. The 24 capacitors with their individual switches and diode clamps are arranged for low inductance connection at the 4 edges of the 90° coil sectors. The method of connection is not shown in the schematic representation of the coil.

11.1.4 Propellant Injector

Details of the propellant injector have not been worked out, but the general approach seems clear. A constant-speed, rotating mechanical shutter would be used to open and close the injection port, thereby avoiding dynamic or bending stresses of any kind.

The shutter might be an annular cylinder with the central volume serving as a plenum. This cylinder would rotate inside a close-fitting sleeve that contained a narrow slit opening into a supersonic nozzle aimed toward the coil. A similar slit in the cylinder would allow gas to pass from the slit in the plenum into the nozzle when it was aligned with the slit in the outer sleeve. At a pulse rate of 30 Hz, for example, and allowing 1 m-sec open time, the ratio of closed time to open time would be 33.

Several of these cylindrical injectors would be arranged end-to-end around the top of the pylon shown in Figure 11.1. Six, forming a hexagon might be enough for azimuthal propellant uniformity.

Figure 11.1(a) shows the thruster from the coil side. The injector nozzle rim is well inside the coil inner radius to avoid impingement of accelerated plasma. As with the previous thrusters, an outer edge barrier prevents loss of propellant during injection.

11.1.5 Thruster Efficiency

A numerical simulation of the PIT has been developed that accurately describes its operation in terms of experimentally determined parameters, (Appendix A). This method has been used to examine the sensitivity of efficiency to these parameters and to estimate the efficiency that might be expected for a large diameter coil. The results are summarized in Figure 11.2 for different values of circuit parasitic inductance L_0, circuit resistance and electron temperature for the 1-meter coil. Also, efficiency is shown as a function of I_{sp} for a 3-meter diameter coil for L_0=0.01 μH, 0.01 Ω external circuit resistance and 3 eV electron temperature. Efficiencies of 54.5% at 2500 seconds I_{sp} and 57.5% at 3000 seconds are shown for the 3 meter coil example. These would be reduced somewhat for the 2 meter coil described earlier

It is instructive to examine the effects of varying the different parameters shown in Figure 11.2 for the 1-meter thruster.

Standard conditions are taken to be: 0.1 μH external inductance, 0.01 Ω external resistance, 3 eV electron temperature and 10^{-5} kg propellant mass. As seen in Figure 11.2, the corresponding performance is 36% efficiency at 1550 seconds I_{sp}. This is a higher efficiency than measured values due, primarily, to non-uniformities in gas density and electron temperature in the experimental thruster. We believe these non-ideal conditions can be reduced so that the performance shown by the numerical simulation can be achieved.

The effect of increasing electron temperature from the standard 3 eV value to 4 eV was to raise the efficiency to 41% at 1650 seconds I_{sp}. At 2 eV the efficiency increased to 27% at 2200 seconds I_{sp}.

Reducing external resistance by one-half has the same effect as reducing the external inductance by one-half. In both cases the efficiency became 39% at 1600 seconds I_{sp}. When the fixed inductance was doubled, to 0.02 μH, the efficiency decreased to 32% at 1450 seconds. Doubling the circuit resistance gave 30% efficiency at 1400 seconds I_{sp}.

This sensitivity map shows the importance of minimizing external circuit resistance and inductance. It is not likely that electron temperature can be increased appreciably. However, the possibility of increasing E_0 by reducing the turns of the drive coil, for a constant propellant mass and bank voltage, may result in some plasma conductivity improvement (higher electron temperature) in the Mark IV thruster.

Three additional cases are shown in Figure 11.2 to illustrate the effects of large reductions in parasitic effects. By eliminating circuit resistance entirely, the efficiency increased to 43% at 1700 seconds I_{sp}. When the plasma resistance was also eliminated, a further increase in efficiency to 64% at 2100 seconds I_{sp} resulted. Finally, with one-tenth of the standard external inductance and no plasma or circuit resistance, the efficiency became 83% at 2250 seconds I_{sp}. These are interesting results, not only because of the high efficiencies calculated for the highly idealized cases but because the much lower values corresponding to experimental conditions are properly accounted for by the numerical simulation. This lends credence to the efficiencies predicted for the large coil.

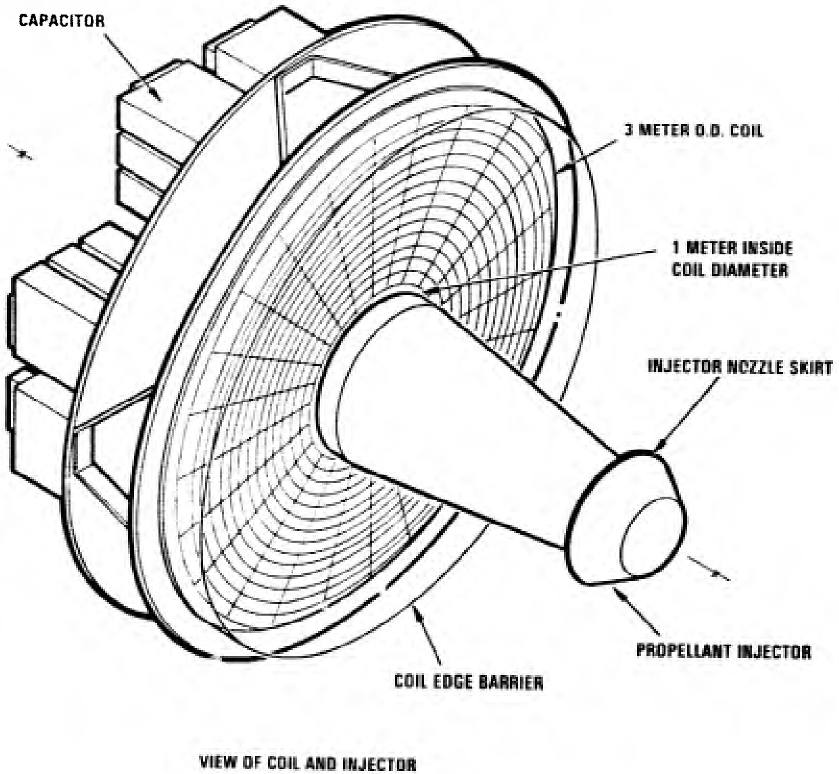

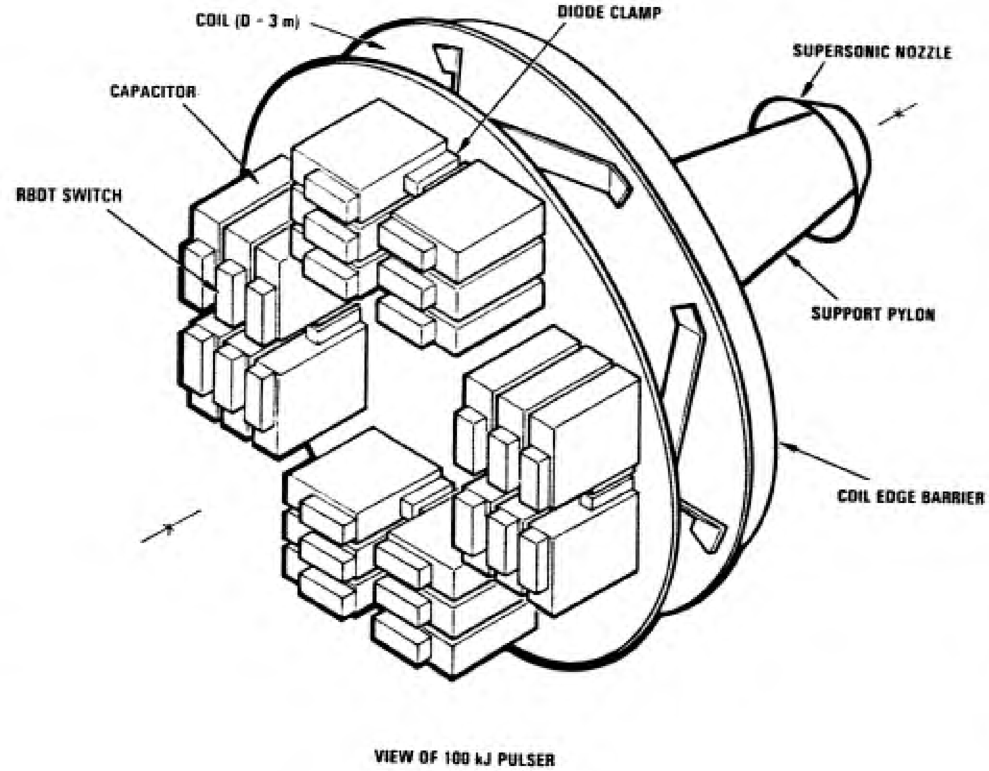

Figure 11.1 Mark IV Type Thruster, Component Arrangement

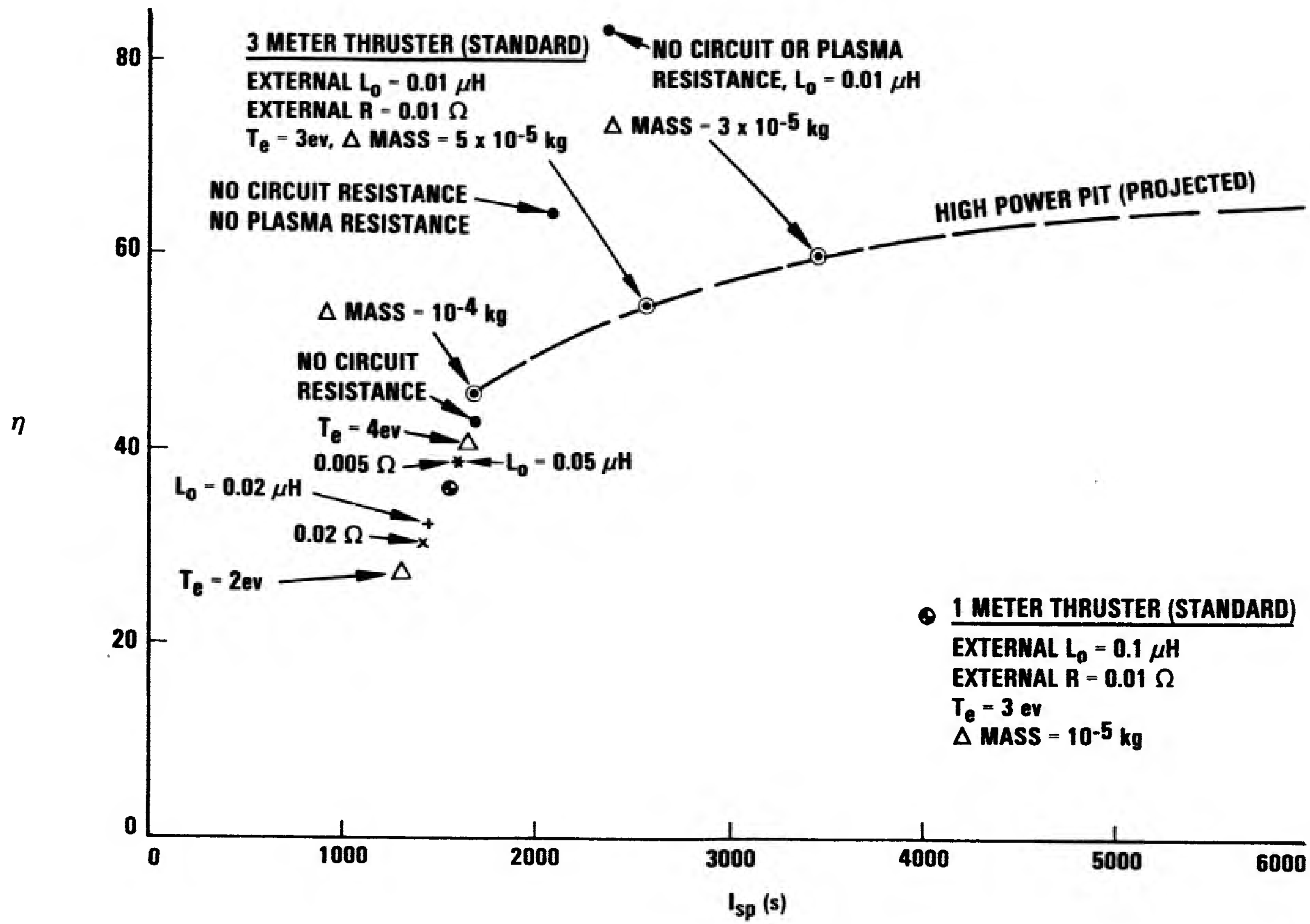

Figure 11.2 Thruster Efficiency for Different Engines

R1/60599-04

REFERENCES

1. I. S. Shpigel, "Plasma Acceleration", Soviet Physics JETP, Vol 36 (9), No. 2, August 1959.

2. L. Hogberg and K. Vogel, "Experiments with Electrodeless Generation and Acceleration", of Plasma Rings", Nuclear Instruments and Methods 10 (1961) 95-107; North Holland Publishing Co., October 1960.

3. Clarence W. Matthews and William Cuddihy, "Experimental Study of a Single-Coil Induced Electromotive Force Plasma Accelerator", NASA TN D-G39, January 1961.

4. Ralph W. Waniek, "Inductive High-Field Plasma Accelerators", ARS Electric Propulsion Conference, March 1962.

5. L. Lindberg, "Experiments With an Electrodeless Plasma Accelerator", Division of Plasma Physics, Royal Institute of Technology, Stockholm 70, Sweden, July 1969.

6. C. Lee Dailey and Ralph H. Lovberg, "Payload Capability and I_{sp} Limitations of High Power Electric Orbit Transfer Vehicles (OTVs)".

7. R. H. Lovberg, B. R. Hayworth and T. Gooding, "The Use of a Coaxial Gun for Plasma Propulsion", G. D. Convair, Rept. AE62-0678, May 1962.

8. R. Jahn, The Physics of Electric Propulsion McGraw-Hill Book Co., New York, 1968, p 269.

9. C. L. Dailey and R. H. Lovberg, "Large Diameter Inductive Plasma Thrusters", AIAA Paper 79-2093, Oct. 1979.

10. J. Marshall, Proc. Second U.N. Int. Conf., Geneva, 1958, Vol 31, p 341.

11. Maxwell Laboratories, private communication.

12. Ralph H. Lovberg and C. Lee Dailey, "Numerical Simulation of Pulsed Inductive Thruster Plasma".

NUMERICAL SIMULATION OF PULSED INDUCTIVE THRUSTER PLASMA

Ralph H. Lovberg*
University of California at San Diego
La Jolla, California
and
C. Lee Dailey**
TRW, STG
Redondo Beach, California

Abstract

The numerical simulation of impulsive plasma acceleration is described for a one-dimensional slab of plasma having density and magnetic field properties similar to those of the TRW pulsed inductive thruster. The results describe the resistive energy loss for different values of plasma resistivity, and compare the total ion kinetic energy with the useful center-of-mass energy. The effect of resistivity is to reduce the impact acceleration loss while increasing the ohmic loss so that an optimum value of resistivity exists for which the acceleration efficiency is actually higher than that for an idealized infinite conductivity plasma. As resistivity is increased, diffusion of the magnetic field through the low density toe of the distribution produces a local velocity that can be several times greater than the center-of-mass velocity; the tenuous plasma is effectively blown away from the current sheet. At the leading edge of this precursor the faster mass elements bunch together in a very thin mass pulse.

Nomenclature

B	magnetic field, Tesla
B_r	radial magnetic field, Tesla
DE	axial kinetic energy, J
E	energy, J
J	plasma current density, amps/m^2
I_{sp}	specific impulse, s
KE	total kinetic energy, J
RE	resistive energy, J
t	time, s
V	axial velocity
Z	axial distance, m
ε	efficiency %
ρ	mass density, kg/m^3
η	resistivity, 1/Ωm

Background

The present experimental program on the 1-meter pulsed inductive thruster at TRW was stimulated by an earlier computer modeling of the system in which the electrical circuits were quite accurately represented and the plasma itself modeled in a very simplified way. In particular, the plasma was assumed to be a simple slab having uniform de sity and constant resistivity. The current layer was taken to be a somewhat thinner uniform slab at the rear of the plasma whose thickness was given by classical diffusion from an assumed initial value. Impact losses due to "snow plowing" were computed on the assumption of zero initial velocity of the plasma and its complete entrainment by the advancing current sheet.

Despite the simplicity of this model, it has provided answers in terms of total impulse, I_{sp}, and efficiency that have agreed quite well with the results of earlier experiments, and have shown as well that thruster efficiency should improve substantially with scale size.[1] The 1-meter thruster experiments have borne out these predictions.

It has seemed, however, that a more accurate modeling of the plasma-field interaction would be valuable both as an aid in interpreting the details of plasma behavior measured in experiments and as a design guide in effecting improvements in performance through adjustments of such parameters as initial gas distribution or composition. Accordingly, we have written a one-dimensional MHD code that provides spatial and temporal distributions of plasma kinetic energy, magnetic field energy, and resistive energy losses.

Details of the Code

The present computation is still approximate to the extent that for the purpose of pressure calculations the plasma is assumed to be isothermal at about 3 ev; multi-electron atoms tend to "thermostat" their plasma temperatures to this region over a wide range of current densities. We also adopt an empirical relation between current density and resistivity, based largely on experimental experience.

Otherwise, we employ the normal set of conservation equations for momentum and mass, the latter following automatically from the use of a Lagrangian mesh. Maxwell's equations are assumed, through the use of the magnetic diffusion equation. Since the resistivity is assumed to depend on current density, the diffusion equation becomes nonlinear so that it has been necessary to employ an iterative implicit scheme for magnetic field calculations. Momentum computations are still done explicitly, however, so in order to satisfy the Courant condition for stability it has been necessary to use time steps as short as two nanoseconds and to superimpose a uniform background density of 1.3×10^{-6} kg/m^3. This density is sufficiently low that it does not significantly affect the results of the computation. The 100 point spatial grid is set at 2 mm intervals between the insulator and a fixed but nonconducting barrier at 20 cm distance. The latter, while artificially confining plasma, does not cause a serious problem, since over the times of interest, no significant motion of the plasma has occurred at this distance; boundary conditions on the mesh are conveniently satisfied by its presence, however.

The initial filling of gas is assumed to be a Gaussian distribution in the axial direction, with maximum at the left-hand insulator at Z = 0. For all of the computations reported here, the 1/e distance was taken to be 6 cm, which is typical of

*Professor of Physics
**Propulsion Staff, Associate Fellow AIAA
†This work was supported by TRW.

measured values.

The electrical driving circuit is not explicitly included in the present work; rather, a particular B(t) is assumed at the insulator. We employ an analytic form that is a good approximation to the B(t) actually observed in experiments.

Computation Results

Comparison with Data

We have run the code for conditions approximating those in the accelerator, so that a comparison can be made with observed parameter distributions. We present a sample computation that is fairly illustrative of the agreement we are able to achieve between theory and experiment.

Figure 1 is a family of measured plots of the radial magnetic field, Br, versus distance along the axial coordinate z for four times during the stroke.

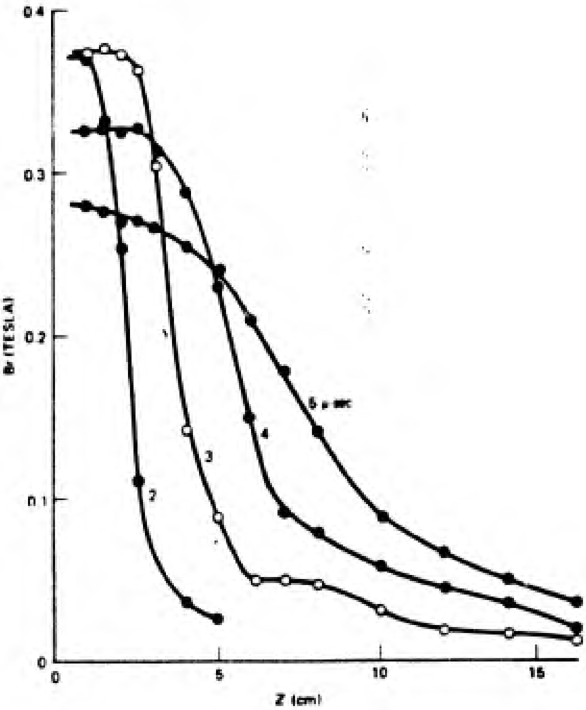

Fig. 1. Experimental Magnetic Field Distribution.

Figure 2 is a computed set, with the initial fill density adjusted to achieve approximately the same axial velocity. It will be noted that while these distributions have strong similarities, there are also significant differences. In particular, the change in slope of $B_r(z)$, or the change in thickness of the current layer, is greater during the actual stroke than during the computed one. The latter does include a current-density-dependent resistivity which should accelerate field diffusion to some degree, but it does not produce quite as rapid a current layer thickening as is observed.

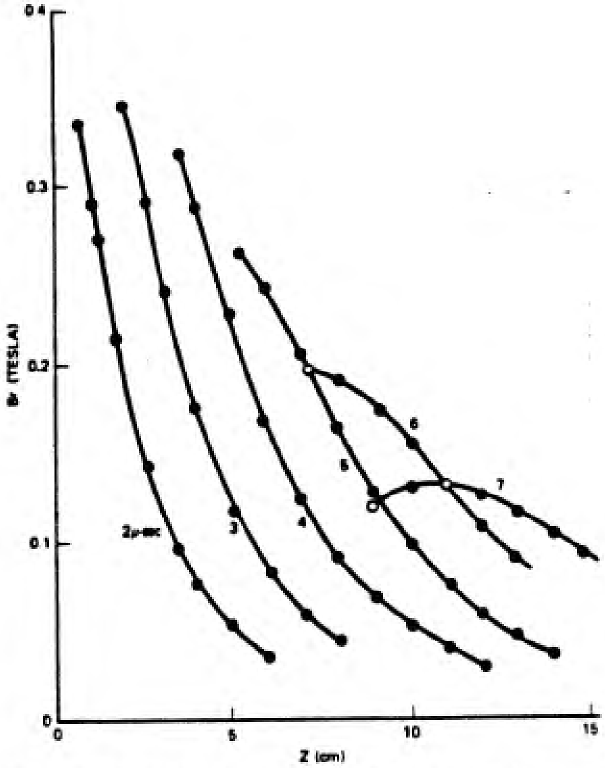

Fig. 2. Computed Magnetic Field Distribution.

The rapid collapse of the B field at 6 and 7 microseconds is the result of the imposed field cycling back toward its half-cycle zero.

Efficiency

Limitation of the efficiency with which a plasma may be impulsively accelerated by a magnetic field occurs in two distinct ways. First, the electrical resistivity of the plasma dissipates field energy heating the plasma and, in our case, producing radiation lines that are mostly in the ultraviolet. Secondly, the motion of the thin current layer or "magnetic piston" at the field-plasma boundary produces impact, or "snowplow," losses as it advances through the stationary gas. [2] The nonuniform acceleration in this instance leaves the plasma with a substantial internal energy. For the case of a piston moving through a uniform plasma, the input work is equally split between internal and translational energies, so the efficiency of acceleration has an upper limit of 50%.

A special property of the acceleration of a plasma slab of finite thickness, however, is that the resistivity of the medium, while producing loss itself, acts to mitigate the loss due to nonuniform acceleration. When the applied magnetic field diffuses resistively through a plasma distribution such as the half-Gaussian assumed in this work, B(z) and ρ(z) tend to assume roughly the same shape, with the result that the plasma accelerations may be fairly uniform along z, or even increase in the forward direction. Impact losses are then much lower than for a uniform density.

In these simulations, we have employed an empirical dependence of resistivity upon current density that is a reasonable approximation to earlier experimental results:

$$\eta = \eta_0/(\log_{10}|J| - 0.5)^{1.5}$$

Space and time distributions of magnetic field, and of density and velocity of the plasma have been computed for four different values of η_0. The plots of Figure 3 show the spatial distribution of B, ρ, and V for $\eta_0 = 3 \times 10^{-4}$, 5×10^{-4}, 10^{-3}, and 2×10^{-3} per Ωm at t = 5 μsec.

It is clear in Fig. 3 that the thickness of the current sheet is greatest for the largest resistivity, as would be expected. One may note also that in case (a), the plasma is compressed into a layer approximately 10 times thinner than that of case (d), and its peak density is correspondingly greater.

The most unusual feature seen in these plots is the velocity distribution. Since B falls off more slowly with z than does the density, we find that the low-density forward toe of ρ(z) becomes strongly accelerated. For the case of the rapid field penetration at highest resistivity, the tenuous forward plasma achieves very high velocity. A further remarkable consequence of this high acceleration is seen in Fig. 4, where ρ(z) is magnified an order of magnitude, and plotted with v(z) at 6 μsec for the resistivity of Fig. 3(d). A very thin mass pulse is seen to develop at the leading edge of the plasma. It results from the bunching of mass elements arriving from the high-acceleration zone just behind it. It seems possible that this forward deflagration of the plasma layer is responsible for the commonly observed production of a very fast and low density precursor to the main plasma emerging from coaxial plasma guns, and also in the inductive accelerator. [3]

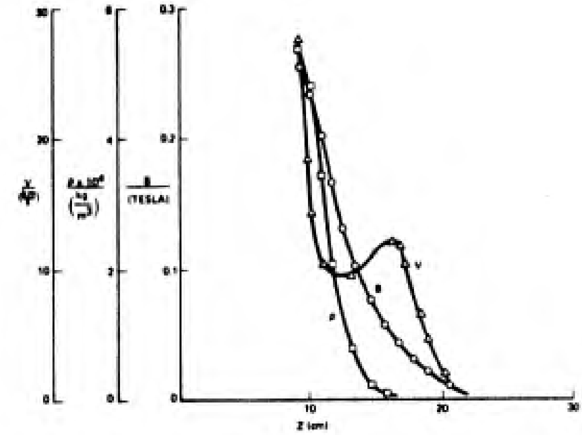

Fig. 3b. ($\eta_0 = 5 \times 10^{-4}$ Ωm)

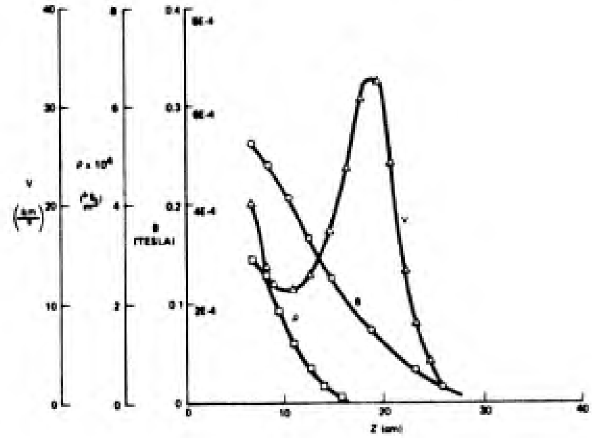

Fig. 3c. ($\eta_0 = 10^{-3}$ Ωm)

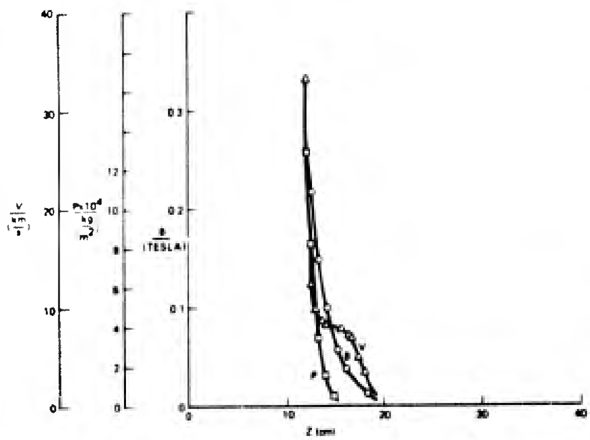

Fig. 3a. ($\eta_0 = 3 \times 10^{-4}$ Ωm)

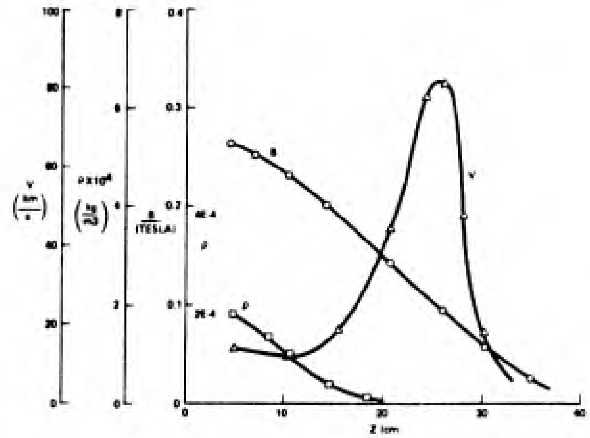

Fig. 3d. ($\eta_0 = 2 \times 10^{-3}$ Ωm)

Fig. 3. Density Velocity and Magnetic Field versus Z at 5 μ-sec.

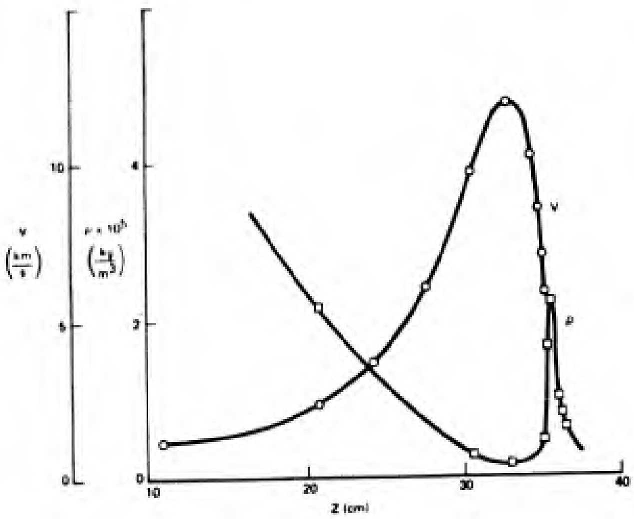

$(\eta_0 = 2 \times 10^{-3}\ \Omega m)$

Fig. 4. Density and Velocity vs Z at = 6 μ-sec.

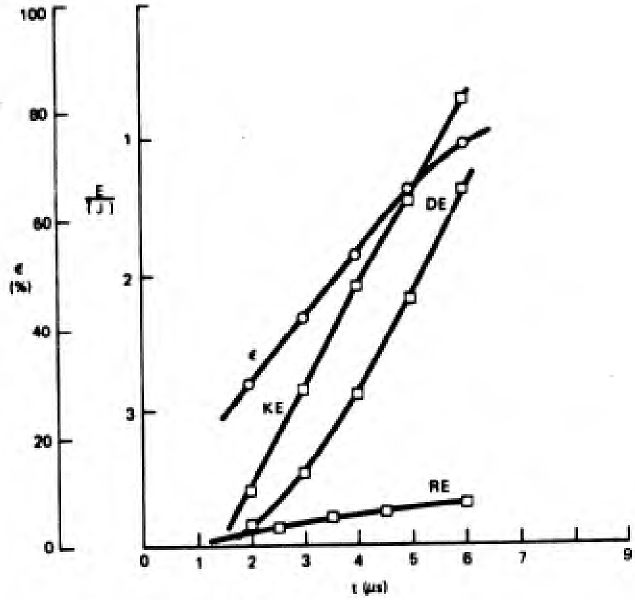

Fig. 5a. $(\eta = 3 \times 10^{-4}\ \Omega)$

Figure 5 shows, for each resistivity, the time history of the total ion kinetic energy, the center-of-mass kinetic energy, the resistance loss and the efficiency, defined as the ratio of center-of-mass energy to the sum of total ion energy and resistance loss. Here, the differential partitioning of resistive and impact losses becomes evident. In case (a), the total ion energy (KE) rises more rapidly than the center-of-mass energy, or directed energy (DE), up to about 4 microseconds after which the difference between them remains nearly constant. This is because impact losses occur early in this case, and the plasma is being accelerated as a "slug" after 4 microseconds. Resistance losses (RE) are relatively small.

In case (b), we see that KE and DE have a much smaller difference. This is due to the somewhat more uniform acceleration of the plasma arising from better field penetration. However, this smaller impact loss is nearly offset by a higher resistance loss. The composite efficiency of case (b), which is a more resistive plasma, is actually the higher of the two over the time interval studied.

The two higher resistivity cases (c and d) exhibit extremely small impact loss up to 5 or 6 microseconds, where it begins to increase. This is not actually due to impact, but rather to deceleration of the rearmost regions of the plasma when the driving magnetic field swings back toward its zero value which occurs at 8 microseconds. The resistive loss for these two cases is quite high, so that their efficiencies finally become low. However, up to 4 microseconds, case (c) is the most efficient of the four.

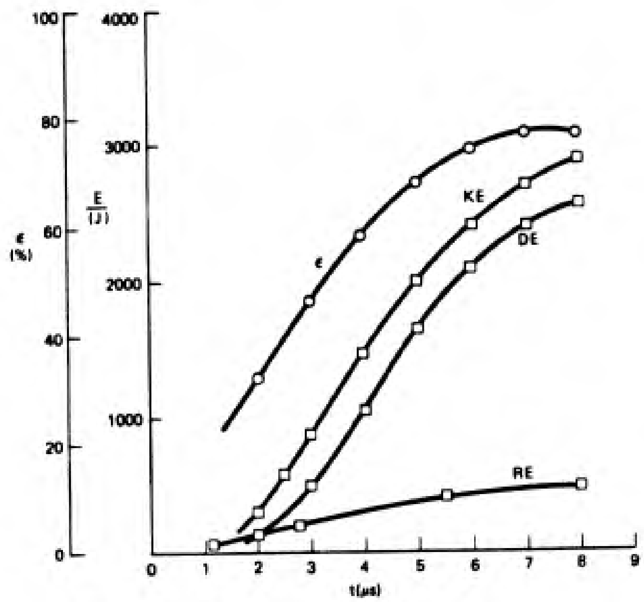

Fig. 5b. $(\eta = 5 \times 10^{-4}\ \Omega m)$

Fig. 5. Comparison of Resistive, Directed and Total Kinetic Energies and Directed Energy Efficiency versus Time.

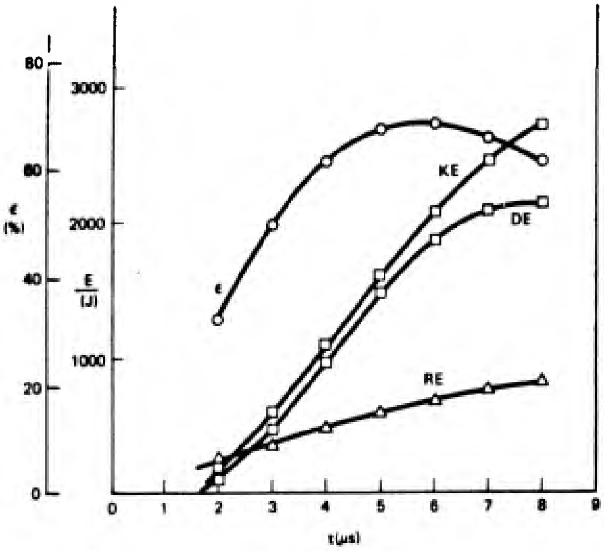

Fig. 5c. ($\eta = 10^{-3}$ Ωm)

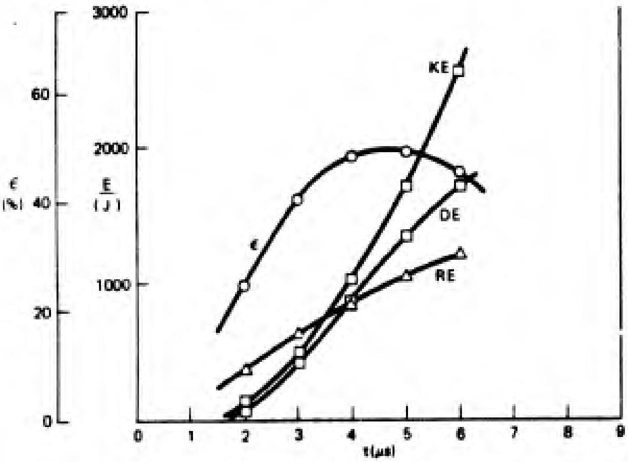

Fig. 5d. ($\eta = 2 \times 10^{-3}$ Ωm)

Fig. 5. Comparison of Resistive, Directed and Total Kinetic Energies and Directed Energy Efficiency versus Time (Continued)

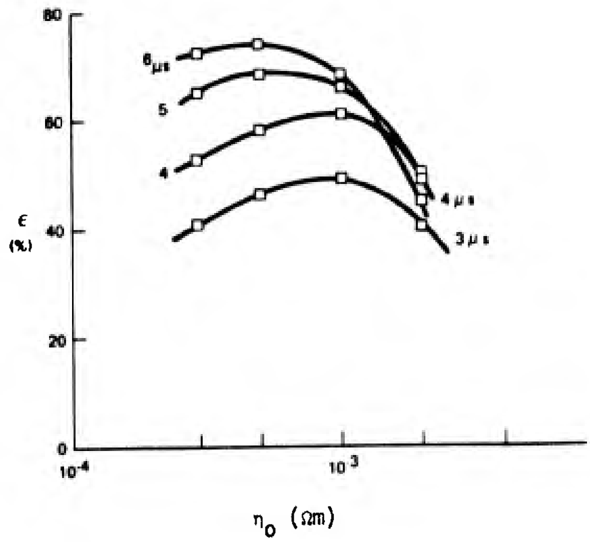

Fig. 6. Efficiency as a Function of Resistivity at Several Times.

Figure 6 presents efficiency as a function of resistivity η_o at several times. We see for example that if, in an actual inductive accelerator, the drive were to end due to decoupling at 3 or 4 microseconds, a plasma resistivity of $\eta_o = 10^{-3}$ ohm-meters is optimum; if longer drive is achieved, a lower plasma resistivity is better.

Acknowledgement

The one-meter thruster, cited in this paper was developed in support of USAF AFRPL Contract F04611-82-C-0058, "Pulsed Inductive Thruster, Comp/Tech". Major G. D. Nordley was the Project Manager.

Conclusion

A one-dimensional computer simulation of the impulsive magnetic acceleration of an isothermal plasma has shown that finite plasma conductivity may actually improve overall acceleration efficiency compared to an idealized infinite conductivity plasma.

References

1. R.H. Lovberg and C.L. Dailey, "Large Inductive Thruster Performance," AIAA Journal, Vol. 20, No. 7, July 1982, p. 971.
2. R. Jahn, The Physics of Electric Propulsion, Mc-Graw-Hill Book Co., New York, 1968, p. 269.
3. C.L. Dailey and R.H. Lovberg, "Current Sheet Structure in an Inductive-Impulsive Plasma Accelerator," AIAA Journal, Vol. 10, No. 2, February 1972, pp. 125-129.